


Article

# Atmosphere-Controlled Solvatomorphic Transitions of Ternary Copper(II) Coordination Compounds in Solid State

Darko Vušak , Matea Primožić and Biserka Prugovečki \*

Department of Chemistry, Faculty of Science, University of Zagreb, Horvatovac 102A, 10000 Zagreb, Croatia; dvusak@chem.pmf.hr (D.V.); matea.primozic@student.pmf.hr (M.P.)

\* Correspondence: biserka@chem.pmf.hr

**Abstract:** Reactions of copper(II) sulfate with 2,2'-bipyridine (bpy) and L-serine (L-Hser) were investigated using different solution-based and mechanochemical methods. Four new ternary coordination compounds were obtained by solution-based synthesis, and three of them additionally via the liquid-assisted mechanochemical method:  $\alpha$ -[Cu(L-Ser)(H<sub>2</sub>O)(bpy)]<sub>2</sub>SO<sub>4</sub> (**1a- $\alpha$** ),  $\beta$ -[Cu(L-Ser)(H<sub>2</sub>O)(bpy)]<sub>2</sub>SO<sub>4</sub> (**1a- $\beta$** ), [Cu(L-Ser)(H<sub>2</sub>O)(bpy)]<sub>2</sub>SO<sub>4</sub>·6H<sub>2</sub>O (**1a·6H<sub>2</sub>O**), and [Cu(L-Ser)(bpy)(CH<sub>3</sub>OH)]<sub>2</sub>SO<sub>4</sub>·2CH<sub>3</sub>OH (**1b·3CH<sub>3</sub>OH**). The compounds were characterized by single-crystal and powder X-ray diffraction, infrared spectroscopy, and thermal analysis. Structural studies revealed two polymorphs (**1a- $\alpha$**  and **1a- $\beta$** ) and two solvatomorphs (**1a·6H<sub>2</sub>O** and **1b·3CH<sub>3</sub>OH**). To investigate the stability of the compounds, crystalline samples were exposed to different conditions of relative humidity (*RH*) and an atmosphere of methanol vapours. Successful solid-state transformation of **1a·6H<sub>2</sub>O** into **1a- $\alpha$**  was established at lower *RH* values, and vice versa at higher *RH* values, while both compounds partially transitioned to **1a- $\beta$**  in the atmosphere of methanol vapours. Compound **1b·3CH<sub>3</sub>OH** decomposed spontaneously into **1a- $\alpha$**  by standing in the air. All of the investigated structural transformations were underpinned with proposed mechanisms. Additionally, **1a- $\alpha$**  showed moderate in vitro antiproliferative activity toward a human breast cancer cell line (MCF-7), a human colon cancer cell line (HCT116), and a human lung cancer cell line (H460).

**Keywords:** biological activity; coordination compounds; crystal structures; crystallization; mechanochemistry; polymorphism; solid-state transformations; solvatomorphism; solvent adsorption; X-ray diffraction



**Citation:** Vušak, D.; Primožić, M.; Prugovečki, B. Atmosphere-Controlled Solvatomorphic Transitions of Ternary Copper(II) Coordination Compounds in Solid State. *Crystals* **2024**, *14*, 986. <https://doi.org/10.3390/cryst14110986>

Academic Editor: Alexander Y. Nazarenko

Received: 26 October 2024

Revised: 11 November 2024

Accepted: 12 November 2024

Published: 15 November 2024



**Copyright:** © 2024 by the authors. Licensee MDPI, Basel, Switzerland. This article is an open access article distributed under the terms and conditions of the Creative Commons Attribution (CC BY) license (<https://creativecommons.org/licenses/by/4.0/>).

## 1. Introduction

Coordination compounds of copper (II) with amino acids and heterocyclic bases have been studied primarily because of their antitumour activity [1–5]. Some of these coordination compounds have been patented as potential antitumour drugs [6]. Additionally, copper coordination compounds have been designed for bioinorganic and medicinal inorganic chemistry applications and used as model compounds for studying the interaction between DNA and proteins [7]. It was found that ternary copper compounds with amino acidates and that heterocyclic bases act against tumour cells either through direct interaction of ternary compounds with DNA, DNA cleavage via reactive oxygen species (ROS) generation, or mitochondrial toxicity [8–11]. Quantitative structure–activity relationship studies on similar ternary copper compounds showed that the presence of phenanthroline was necessary to preserve the antiproliferative activity and that the nature of the *O,N* ligand had a minor influence on biological activity [12].

Among the published crystal structures of copper(II) with amino acid and heterocyclic bases that are derivatives of 2,2'-bipyridine (bpy), crystal structures with 2,2'-bipyridine and 1,10-phenanthroline (phen) predominate [13]. Different structures can be attained by various synthetic approaches, most commonly by solution-based methods. Another means of producing different architectures is by solid-state transformation. Generally,

such transformations are more challenging to achieve than those in solutions but minimize energy consumption and waste production while adhering to the principles of green chemistry [14,15]. In recent decades, mechanochemistry became more popular method for synthesis of different kinds of materials, such as cocrystals, metal–organic frameworks, and organic compounds, sometimes yielding products that are difficult to obtain from solution [14,16–18]. In the solid-state chemistry of coordination compounds, solvent molecules can drive reactions towards different products, depending on the type and amount of solvent [17,19].

Compounds that contain a copper ion, an amino acid, and a heterocyclic base 2,2'-bipyridine in their structure are most often discrete coordination compounds (0D) in which the amino acid coordinates the metal through the carboxylate oxygen and nitrogen from the amino group and 2,2'-bipyridine serves as a bidentate ligand coordinating Cu through nitrogen atoms [20–22]. In some cases, the carboxylate group and the functional group from the amino acid's side chain can coordinate the neighbouring copper ions, thus increasing the dimensionality from 0D to 1D chains [1,23–25]. Changing the type of ligands, i.e., amino acids and heterocyclic bases, leads to different architectures based on hydrogen bonds and  $\pi$ -interactions. Most of the published crystal structures of copper(II) ternary coordination compounds with amino acids and heterocyclic bases contain water molecules and, in several structures, small alcohols (coordinated and/or crystallization). Such complexes containing additional hydrogen bond donors and/or acceptors can form porous structures where solvent molecules form 0D pockets, 1D chains, or 2D frameworks. Porous compounds can also recognize and adsorb solvent/other guest molecules, which gives them potential application as catalysts or in solvent/gas storage and separation [26–31]. Moreover, ternary coordination compounds of copper(II), heterocyclic bases, and amino acidates are potential ferroelectric materials [32]. In the CSD database, there are 57 datasets of compounds containing copper(II), amino acidates, and 2,2'-bipyridine, none of which contain L-serinate [13].

Our main interest is to investigate biocompatible materials and their properties in the solid state. Polymorphism and solvatomorphism are of great importance today for the design of new architectures of crystalline compounds and targeted tuning of their properties, especially in the fields of material and pharmaceutical science [33–35]. In the pharmaceutical industry, polymorphism and solvatomorphism can have substantial medical (different physical, chemical, or biological) properties, as well as regulatory implications [36,37]. For any practical application, it is important to investigate optimal synthetic conditions, as well as the stability and properties of the targeted material. The composition of the atmosphere (humidity, partial pressures of solvent vapours or gases) and some external conditions, such as temperature and pressure, can influence the structure of a material, which could lead to undesired changes in material properties. Structural transformations of compounds in the solid state can be interesting information for theoretical investigations of solid-state reactions and interconversions, and ultimately for the prediction of the crystal structure of reaction products [38,39].

Recently, we reported syntheses, structures, and magnetic and biological properties of a series of ternary copper(II) coordination compounds with amino acids (glycine, L-alanine, L-valine, L-phenylalanine) and 2,2'-bipyridine [40,41]. In this work, we investigated copper(II) sulfate reactions with 2,2'-bipyridine (bpy) and L-serine under different solution-based and mechanochemical synthetic methods. Four new monomeric ternary copper(II) compounds with 2,2'-bipyridine (bpy) and L-serine (L-Hser) were prepared:  $\alpha$ -[Cu(L-ser)(H<sub>2</sub>O)(bpy)]<sub>2</sub>SO<sub>4</sub> (**1a- $\alpha$** ),  $\beta$ -[Cu(L-ser)(H<sub>2</sub>O)(bpy)]<sub>2</sub>SO<sub>4</sub> (**1a- $\beta$** ), [Cu(L-ser)(H<sub>2</sub>O)(bpy)]<sub>2</sub>SO<sub>4</sub>·6H<sub>2</sub>O (**1a·6H<sub>2</sub>O**), and [Cu(L-ser)(bpy)(CH<sub>3</sub>OH)]<sub>2</sub>SO<sub>4</sub>·3CH<sub>3</sub>OH (**1b·3CH<sub>3</sub>OH**). Two polymorphs and two solvatomorphs were obtained. To investigate the stability of said compounds, they were exposed to different conditions of relative humidity and an atmosphere of methanol vapours (at 20 °C). Compound **1a·6H<sub>2</sub>O** was successfully transformed into **1a- $\alpha$**  at lower relative humidities, and vice versa at high relative humidities, while in the atmosphere of methanol vapours, both **1a·6H<sub>2</sub>O** and **1a- $\alpha$**  partially transitioned to **1a- $\beta$** .

## 2. Materials and Methods

All chemicals, copper(II) sulfate pentahydrate (Gram-Mol, Zagreb, Croatia), copper(II) hydroxide (Alfa Aesar, Ward Hill, MA, USA), 2,2'-bipyridine (Acros Organics, Geel, Belgium), L-serine (TCI, Tokyo, Japan), methanol (Gram-Mol, Zagreb, Croatia), pyridine (Carlo Erba Reagents, Milano, Italy), phosphorous(V) oxide (Acros Organics, Geel, Belgium), sodium hydroxide (Carlo Erba Reagents, Milano, Italy), potassium acetate (Kemika, Zagreb, Croatia), magnesium chloride hexahydrate (Kemika, Zagreb, Croatia), potassium carbonate (Fischer Scientific, Pittsburgh, PA, USA), magnesium nitrate (Merck, Darmstadt, Germany), cobalt(II) chloride hexahydrate (Kemika, Zagreb, Croatia), sodium chloride (Alkaloid, Skopje, North Macedonia), ammonium chloride (Kemika, Zagreb, Croatia), potassium chloride (Zorka Sabac, Sabac, Serbia), and potassium nitrate (Alkaloid, Skopje, North Macedonia), were used without further purification. Anhydrous  $\text{CuSO}_4$ ,  $\text{CuSO}_4 \cdot \text{H}_2\text{O}$ , and  $\text{CuSO}_4 \cdot 3\text{H}_2\text{O}$  were prepared by heating  $\text{CuSO}_4 \cdot 5\text{H}_2\text{O}$  at different temperatures (220 °C, 120 °C, and 60 °C, respectively). The purity of copper(II) sulfate hydrates was confirmed by powder X-ray diffraction. Powder X-ray diffraction (PXRD) was measured on Malvern PANalytical AERIS in the Bragg–Brentano geometry using  $\text{CuK}\alpha$  radiation ( $\lambda = 1.54056 \text{ \AA}$ ) at room temperature. Powder samples were placed on the zero-background silicon holder. Diffraction patterns were measured in the range of  $2\theta = 5\text{--}40^\circ$  with  $0.022^\circ$  and at 15.045 s per step. PXRD data were analysed and visualized using the HighscorePlus suite, version 5.2 and DataViewer, version 1.9a [42,43].

For thermogravimetric analysis, a Mettler Toledo TGA/DSC 3+ was used under an oxygen flow of  $50 \text{ mL min}^{-1}$  and a heating rate of  $10 \text{ }^\circ\text{C min}^{-1}$  in the 25–800 °C temperature range. The sample (approximately 9.0 mg) was placed in a standard alumina crucible. IR(ATR) spectrum was measured using a Thermo Scientific™ Nicolet™ iS50 FTIR Spectrometer in ATR mode at  $4000\text{--}400 \text{ cm}^{-1}$ .

Mechanochemical syntheses were performed on a Retsch MM200 grinder operating at a frequency of 25 Hz for 15 min.

### 2.1. Synthetic Procedures

#### 2.1.1. Solution-Based Syntheses

**Synthesis of  $\alpha\text{-}[\text{Cu}(\text{L-ser})(\text{H}_2\text{O})(\text{bpy})_2]\text{SO}_4$  (**1a- $\alpha$** ).** Anhydrous copper(II) sulfate (39.9 mg, 0.25 mmol), 2,2'-bipyridine (78.1 mg, 0.50 mmol), L-serine (52.7 mg, 0.50 mmol), copper(II) hydroxide (24.4 mg, 0.25 mmol), and methanol (10 mL) were mixed and heated in a beaker at the boiling temperature for an hour and allowed to cool to room temperature. Light blue crystals of  $[\text{Cu}(\text{SO}_4)(\text{bpy})_2] \cdot \text{CH}_3\text{OH}$  (CSD refcode OREGY, [44]) formed. After a few days, the light blue crystals disappeared and dark blue crystals of **1a- $\alpha$**  suitable for single-crystal X-ray structure analysis formed. Additionally, **1a- $\alpha$**  crystallized if pyridine (10 mL) or a mixture of pyridine and methanol was used as a solvent (9:1 or 5:5 *v/v*, 10 mL). **1a- $\alpha$**  crystallizes with some impurities, and it is difficult to crystallize it in a pure form. In all synthetic procedures, heating was needed to accelerate reactions. Mechanochemical synthesis was shown as a better method for obtaining pure compound.

IR (ATR) for **1a- $\alpha$** :  $\tilde{\nu}/\text{cm}^{-1}$ : 3433 (m), 3206 (s), 3112 (s), 3079 (s), 3064 (s), 3037 (s), 2941 (m), 2878 (m), 1626 (s), 1601 (s), 1498 (w), 1477 (m), 1444 (s), 1399 (s), 1353 (m), 1318 (m), 1253 (w), 1175 (m), 1160 (m), 1059 (s), 1030 (s), 1018 (s), 969 (m), 922 (w), 904 (w), 877 (w), 857 (w), 801 (m), 771 (s), 730 (s), 655 (m), 638 (m), 598 (s), 548 (m), 417 (m), 410 (w).

**Synthesis of  $[\text{Cu}(\text{L-ser})(\text{H}_2\text{O})(\text{bpy})_2]\text{SO}_4 \cdot 6\text{H}_2\text{O}$  (**1a-6H<sub>2</sub>O**).** Copper(II) sulfate pentahydrate (62.4 mg, 0.25 mmol), 2,2'-bipyridine (78.1 mg, 0.50 mmol), L-serine (52.5 mg, 0.50 mmol), copper(II) hydroxide (24.4 mg, 0.25 mmol), and water (10 mL) were mixed and heated in a beaker for 15 min at the boiling temperature. The solution was quickly evaporated to one-third of the starting volume, and blue crystals of **1a-6H<sub>2</sub>O** were formed, suitable for single-crystal X-ray diffraction. The same compound crystallized if **1a- $\alpha$**  had been dissolved in water and the solution evaporated at room temperature. If the solution was left in a closed container for several days and then evaporated, light blue crystals of  $[\text{Cu}(\mu\text{-ox})(\text{bpy})_2] \cdot 2\text{H}_2\text{O}$  (CSD refcode BISWOP, [45]) or dark blue crystals of

$\{[\text{Cu}(\text{H}_2\text{O})(\text{bpy})]_2(\mu\text{-ox})[\text{Cu}(\text{ox})(\text{bpy})]\text{SO}_4\}_n \cdot 2\text{H}_2\text{O}$  (CSD refcode JINWOS, [46]) started to form. Crystals of **1a·6H<sub>2</sub>O** are not stable outside of the solution and start to decompose.

**Synthesis of  $\beta$ -[Cu(L-ser)(H<sub>2</sub>O)(bpy)]<sub>2</sub>SO<sub>4</sub> (1a- $\beta$ ) and [Cu(L-ser)(bpy)(CH<sub>3</sub>OH)]<sub>2</sub>SO<sub>4</sub>·3CH<sub>3</sub>OH (1b·3CH<sub>3</sub>OH).** Anhydrous copper(II) sulfate (79.8 mg, 0.50 mmol), 2,2'-bipyridine (78.1 mg, 0.50 mmol), L-serine (52.5 mg, 0.50 mmol), sodium hydrogen carbonate (42.0 mg, 0.50 mmol), and methanol (10 mL) were mixed in a Teflon-lined stainless-steel autoclave for 30 min at 120 °C. After cooling the reaction mixture, two types of blue needles were formed, indistinguishable by their colour (or shade of blue) or habitus. Crystals of **1a- $\beta$**  are stable at room temperature outside of solution, while crystals of **1b·3CH<sub>3</sub>OH** decompose in seconds. The difference in stabilities enabled us to distinguish between the two compounds and analyse both of them by single-crystal X-ray diffraction. In some experiments, only **1b·3CH<sub>3</sub>OH** was formed using the same procedure.

**Synthesis of [Cu(L-ser)(bpy)(CH<sub>3</sub>OH)]<sub>2</sub>SO<sub>4</sub>·3CH<sub>3</sub>OH (1b·3CH<sub>3</sub>OH).**

Anhydrous copper(II) sulfate (39.9 mg, 0.25 mmol), 2,2'-bipyridine (78.1 mg, 0.50 mmol), L-serine (52.6 mg, 0.50 mmol), copper(II) hydroxide (24.4 mg, 0.25 mmol), pyridine (1 mL), and methanol (9 mL) were mixed and heated in a beaker for 15 min at the boiling temperature. After cooling to room temperature, large, dark blue crystals of **1b·3CH<sub>3</sub>OH**, suitable for single-crystal X-ray diffraction analysis, were formed. Crystals decomposed when taken out of the solution. Smaller crystals of the same compound were formed using the same reactants, dissolved in only methanol (10 mL), and heated in an autoclave for 30 min at 120 °C. If the resulting methanolic solution was quickly evaporated at room temperature, blue crystals of **1a- $\alpha$**  were formed. In some repeated syntheses, light blue crystals of [Cu(SO<sub>4</sub>)(bpy)<sub>2</sub>]·CH<sub>3</sub>OH (CSD refcode OREGY, [44]) also formed.

### 2.1.2. Mechanochemical Syntheses

**General procedure for the mechanochemical synthesis of 1a- $\alpha$ , 1a·6H<sub>2</sub>O, and 1b·3CH<sub>3</sub>OH.** Syntheses were performed using the neat grinding (NG) and liquid-assisted grinding (LAG) methods using water and/or methanol. To explore solvation space in more detail, we used various hydrates of copper(II) sulfate and different liquids for the LAG method. L-Serine (0.50 mmol), 2,2'-bipyridine (0.50 mmol), copper(II) hydroxide (0.25 mmol), various hydrates of copper(II) sulfate (pentahydrate, trihydrate, monohydrate, anhydrous; 0.25 mmol), and a small amount of water/methanol were placed in a Teflon milling jar (volume 14 mL). Milling was performed at room temperature for 15 min using one stainless-steel ball (diameter 8 mm). **1a·6H<sub>2</sub>O** was synthesized only if one of the reactants was copper(II) sulfate pentahydrate, with added water ( $\eta = 0.2$  and  $0.1 \mu\text{L mg}^{-1}$ ). **1b·3CH<sub>3</sub>OH** was synthesized only with a large amount of methanol added to the reaction mixture ( $\eta = 1.8 \mu\text{L mg}^{-1}$ ). **1a- $\alpha$**  was formed in most synthetic conditions. Neat grinding led to no reaction if other hydrates (except for pentahydrate) or anhydrous copper(II) sulfate were used. The details of the experimental data and the products are given in Tables S1–S3. Products of mechanochemical syntheses were analysed by powder X-ray diffraction (Figures S1–S19).

### 2.2. Solvent Exchange Experiments

**Aging in Methanol Vapour.** Samples of **1a·6H<sub>2</sub>O** and **1a- $\alpha$**  were placed into a small container with a methanol vapour atmosphere at a constant temperature of 20 °C. Structural changes of samples were monitored ex situ by PXRD, collecting diffraction patterns after one, two, four, and eight weeks.

**Interconversion 1a·6H<sub>2</sub>O  $\rightleftharpoons$  1a- $\alpha$ .** Samples of **1a·6H<sub>2</sub>O** and **1a- $\alpha$**  were placed in containers with water ( $RH = 100\%$ ), phosphorus(V) oxide ( $RH \approx 0\%$ ), and saturated solutions of various inorganic compounds with fixed relative humidity: potassium nitrate ( $RH = 95\%$ ), potassium chloride ( $RH = 85\%$ ), ammonium chloride ( $RH = 79\%$ ), sodium chloride ( $RH = 75\%$ ), cobalt(II) chloride ( $RH = 65\%$ ), magnesium nitrate ( $RH = 54\%$ ), potassium carbonate ( $RH = 43\%$ ), magnesium chloride ( $RH = 33\%$ ), potassium acetate ( $RH = 23\%$ ), and sodium hydroxide ( $RH = 9\%$ ) [47]. Structural changes of samples were monitored ex situ by PXRD, collecting diffraction patterns after one, two, and four weeks. No significant

changes were observed in PXRD patterns after one week. PXRD patterns after 4 weeks of aging of **1a·6H<sub>2</sub>O** (Figure S20) and **1a-α** (Figure S21) are given in Supplementary Materials. The experiment was performed in a temperature-controlled laboratory at 20 °C.

### 2.3. Single-Crystal X-Ray Diffraction

#### 2.3.1. Data Collection and Refinement

Single-crystal X-ray diffraction data of **1a·6H<sub>2</sub>O**, **1a-α** and **1b·3CH<sub>3</sub>OH** were collected on an Elettra Sincrotrone Trieste facility on XRD1 and XRD2 beamlines at 100 K. The wavelength of the measurement was set to 0.700 Å. X-ray diffraction data for **1a-β** were collected on a Rigaku XtaLAB Synergy-S diffractometer equipped with a HyPix 6000HE detector using CuK<sub>α</sub> radiation ( $\lambda = 1.54056$  Å) at 100 K. The diffraction data were processed using the CrysAlisPRO software, version 171.42.63a [48]. Crystal structures were solved by SHELXS (version 2013/1) [49] and refined by the SHELXL (version 2018/3) [50] software incorporated in the WinGX software package, version 2023.1 [51]. The structures were visualized by the Mercury program (version 2024.1.0) [52]. Geometrical parameters were calculated by PLATON (version v1.17) [53], and the simplification of hydrogen bonding was performed by ToposPro (version 5.5.2.2) [54]. Hirshfeld surface analysis was performed by the CrystalExplorer program (version 21.5) [55]. All nonhydrogen atoms were refined anisotropically. Hydrogen atoms were located in the Fourier difference map, but because of the poor geometry of some of them, we placed most of the hydrogen atoms on calculated positions according to idealized geometry. Hydrogen atoms of water and some hydrogen atoms of methanol (in hydroxyl groups) molecules were located in the Fourier difference map. Hydrogen atoms that belonged to water molecules were restrained to an O–H distance of 0.85(1) Å and H–H distance of 1.39(2) Å. Hydrogen atoms of hydroxyl groups of three methanol molecules in **1b·3CH<sub>3</sub>OH** were found in the Fourier difference map and restrained to an O–H distance of 0.84(1) Å. The hydroxyl group of the L-serinato ligands in one of the symmetrically independent cations in **1a-α** and **1a-β** was disordered over two positions. Occupancies of hydroxyl groups were refined to values of 0.34091:0.65909 (in **1a-α**) and 0.61126:0.38874 (in **1a-β**), with a total occupancy factor constrained to 1. Crystallographic data for **1a·6H<sub>2</sub>O**, **1a-α**, **1a-β**, and **1b·3CH<sub>3</sub>OH** are given in Table S4 in the Supplementary Materials.

#### 2.3.2. Crystal Structure Data

Crystal data for **1a-α**, C<sub>26</sub>H<sub>32</sub>Cu<sub>2</sub>N<sub>6</sub>O<sub>12</sub>S ( $M = 779.71$  g/mol): monoclinic, space group  $P2_1$  (no. 4),  $a = 7.1389(1)$  Å,  $b = 20.7625(4)$  Å,  $c = 20.0048(4)$  Å,  $\beta = 95.348(2)^\circ$ ,  $V = 2952.23(9)$  Å<sup>3</sup>,  $Z = 4$ ,  $T = 100(2)$  K,  $\mu(\text{sync}) = 1.455$  mm<sup>-1</sup>,  $D_{\text{calc}} = 1.754$  g/cm<sup>3</sup>, 11,978 reflections measured ( $4.0^\circ \leq 2\Theta \leq 51.8^\circ$ ), 11,978 unique ( $R_{\text{int}} = 0.0743$ ,  $R_{\text{sigma}} = 0.0551$ ), which were used in all calculations. The final  $R_1$  was 0.0673 ( $I > 2 \sigma(I)$ ), and  $wR_2$  was 0.1637 (all data).

Crystal data for **1a-β**, C<sub>26</sub>H<sub>32</sub>Cu<sub>2</sub>N<sub>6</sub>O<sub>12</sub>S ( $M = 779.71$  g/mol): monoclinic, space group  $P2_1$  (no. 4),  $a = 10.0790(3)$  Å,  $b = 20.9260(5)$  Å,  $c = 14.5656(3)$  Å,  $\beta = 107.209(3)^\circ$ ,  $V = 2934.55(14)$  Å<sup>3</sup>,  $Z = 4$ ,  $T = 100(2)$  K,  $\mu(\text{CuK}\alpha) = 3.129$  mm<sup>-1</sup>,  $D_{\text{calc}} = 1.765$  g/cm<sup>3</sup>, 79,459 reflections measured ( $6.4^\circ \leq 2\Theta \leq 136.4^\circ$ ), 10,665 unique ( $R_{\text{int}} = 0.1476$ ,  $R_{\text{sigma}} = 0.0587$ ), which were used in all calculations. The final  $R_1$  was 0.0620 ( $I > 2 \sigma(I)$ ), and  $wR_2$  was 0.1561 (all data).

Crystal data for **1a·6H<sub>2</sub>O**, C<sub>26</sub>H<sub>44</sub>Cu<sub>2</sub>N<sub>6</sub>O<sub>18</sub>S ( $M = 887.81$  g/mol): monoclinic, space group  $P2_1$  (no. 4),  $a = 6.7125(1)$  Å,  $b = 20.8435(2)$  Å,  $c = 13.1341(1)$  Å,  $\beta = 103.455(1)^\circ$ ,  $V = 1787.18(4)$  Å<sup>3</sup>,  $Z = 2$ ,  $T = 100(2)$  K,  $\mu(\text{sync}) = 1.221$  mm<sup>-1</sup>,  $D_{\text{calc}} = 1.650$  g/cm<sup>3</sup>, 19,816 reflections measured ( $3.2^\circ \leq 2\Theta \leq 60.0^\circ$ ), 10,178 unique ( $R_{\text{int}} = 0.0358$ ,  $R_{\text{sigma}} = 0.0360$ ), which were used in all calculations. The final  $R_1$  was 0.0335 ( $I > 2 \sigma(I)$ ), and  $wR_2$  was 0.0937 (all data).

Crystal data for **1b·3CH<sub>3</sub>OH**, C<sub>31</sub>H<sub>48</sub>Cu<sub>2</sub>N<sub>6</sub>O<sub>15</sub>S ( $M = 903.89$  g/mol): orthorhombic, space group  $P2_12_12_1$  (no. 19),  $a = 6.8675(1)$  Å,  $b = 20.9159(2)$  Å,  $c = 26.4444(3)$  Å,  $V = 3798.47(8)$  Å<sup>3</sup>,  $Z = 4$ ,  $T = 100(2)$  K,  $\mu(\text{sync}) = 1.203$  mm<sup>-1</sup>,  $D_{\text{calc}} = 1.581$  g/cm<sup>3</sup>, 63,205 reflections measured ( $3.6^\circ \leq 2\Theta \leq 60.0^\circ$ ), 11,541 unique ( $R_{\text{int}} = 0.123$ ,  $R_{\text{sigma}} = 0.0479$ ), which were used in all calculations. The final  $R_1$  was 0.0496 ( $I > 2 \sigma(I)$ ), and  $wR_2$  was 0.1349 (all data).

#### 2.4. Antiproliferation Assays

The experiments were carried out on three human cell lines derived from three cancer types: H460 (lung carcinoma), MCF-7 (breast carcinoma), and HCT116 (colon carcinoma), in line with previously published experimental procedures [56,57]. H460, MCF-7, and HCT116 cells were cultured as monolayers and maintained in Dulbecco's modified Eagle medium (DMEM), supplemented with 10% foetal bovine serum (FBS), 2 mM L-glutamine, 100 U/mL penicillin, and 100 µg/mL streptomycin in a humidified atmosphere with 5% CO<sub>2</sub> at 37 °C.

The cells were seeded on standard 96-well microtiter plates and allowed to attach for 24 h. The next day, the test compound was added in five serial 10-fold dilutions. Cell viability was assessed after 72 h of incubation using the MTT assay, which detects dehydrogenase activity in viable cells. The MTT assay is a colorimetric assay system that measures the reduction of a tetrazolium component (MTT) into an insoluble formazan product by the mitochondria of viable cells. The absorbance (optical density, OD), measured on a microplate reader at 570 nm, is directly proportional to cell viability. The percentage of growth (PG) of the cell lines was calculated. The results obtained are expressed as an IC<sub>50</sub> value, which represents the concentration of the compound that caused 50% growth inhibition. The IC<sub>50</sub> values were calculated from the concentration–response curve using linear regression analysis by adjusting the test concentrations giving PG values above and below the reference value (i.e., 50%). If all tested concentrations resulted in PG values above the corresponding reference value, the highest tested concentration was marked with a “>” sign as the default value. Each test was performed in quadruplicate in at least two individual tests.

### 3. Results

#### 3.1. Syntheses and Crystallizations

Solution-based (Figure 1) and mechanochemical methods (Figure 2) were utilized for the syntheses of four new ternary coordination compounds of copper(II) with L-serine (L-Hser) and 2,2'-bipyridine (bpy), and all were structurally characterized. A total of four reactants were used in reactions: anhydrous or different hydrates of copper(II) sulfate (monohydrate, trihydrate, pentahydrate), copper(II) hydroxide or sodium hydrogen carbonate, 2,2'-bipyridine, and L-serine. **1a·6H<sub>2</sub>O** was obtained from a solution containing only water as a solvent, from a reaction, or by recrystallization of **1a-α** from water. In most of the explored conditions (various solvents and hydrates of copper(II) sulfate), **1a-α** crystallized. In most experiments, crystals of **1a-α** did not have good quality for single-crystal X-ray analysis, so synchrotron radiation was needed. Using anhydrous copper(II) sulfate and at low water and high methanol fraction in solution, **1a-β** (polymorph of **1a-α**) and **1b·3CH<sub>3</sub>OH** crystallized, often along with [Cu(SO<sub>4</sub>)(bpy)<sub>2</sub>]**·CH<sub>3</sub>OH**. **1a-β** is difficult to crystallize, and it does not always form in repeated experiments, which indicates that it is stable or metastable only in a narrow range of conditions, while **1b·3CH<sub>3</sub>OH** formed always from solutions with a high fraction of methanol, as specified in the experimental section. In all solution-based experiments, a crucial step for the successful isolation of compounds was quick crystallization, because compounds are unstable in solution. It seems that these coordination compounds are catalysts for the oxidation of amino acids into oxalate ions, since oxalate complexes crystallized after several days.

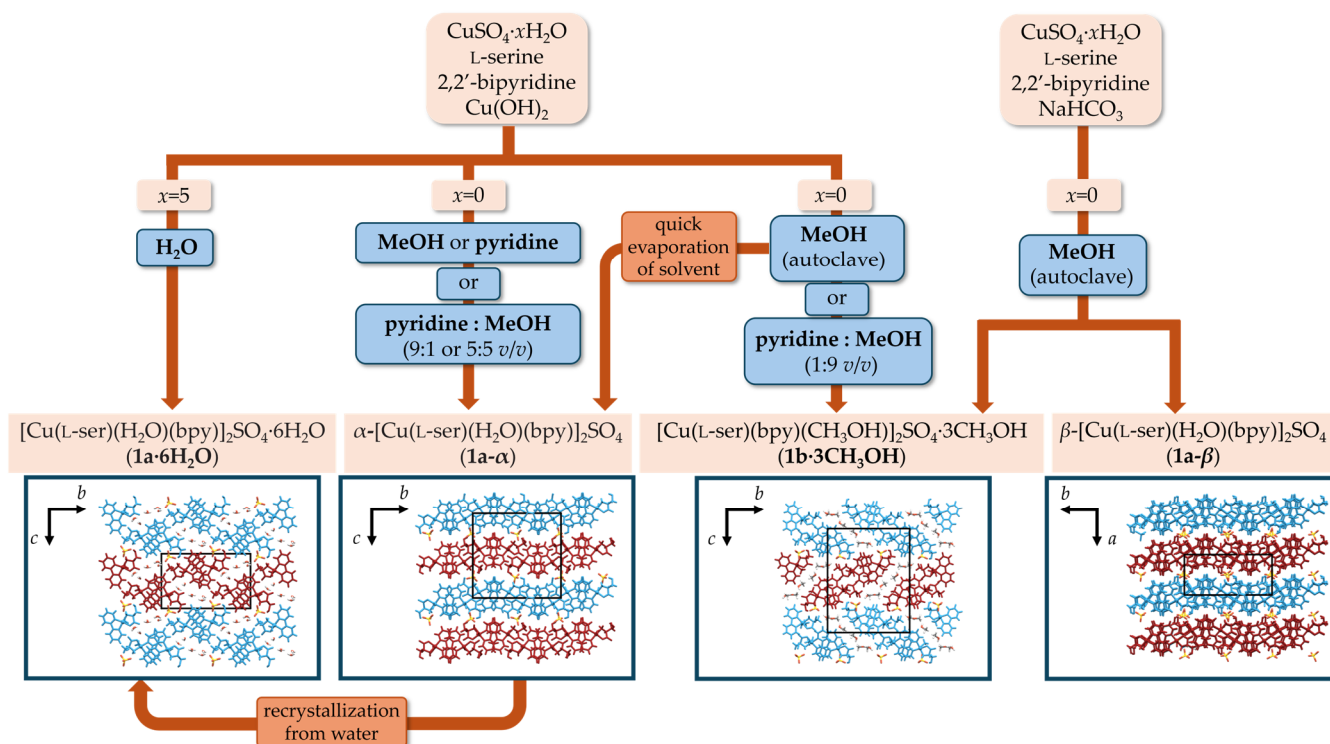


**Figure 1.** Schematic diagram of solution-based syntheses and the main products. As stated in the Materials and Methods section, some byproducts also formed in the syntheses and were omitted from the scheme for clarity. Differences in crystal packings of unit cells of all four compounds are shown. Layers of complexes of different colours (blue and red) are separated by sulfate ions.

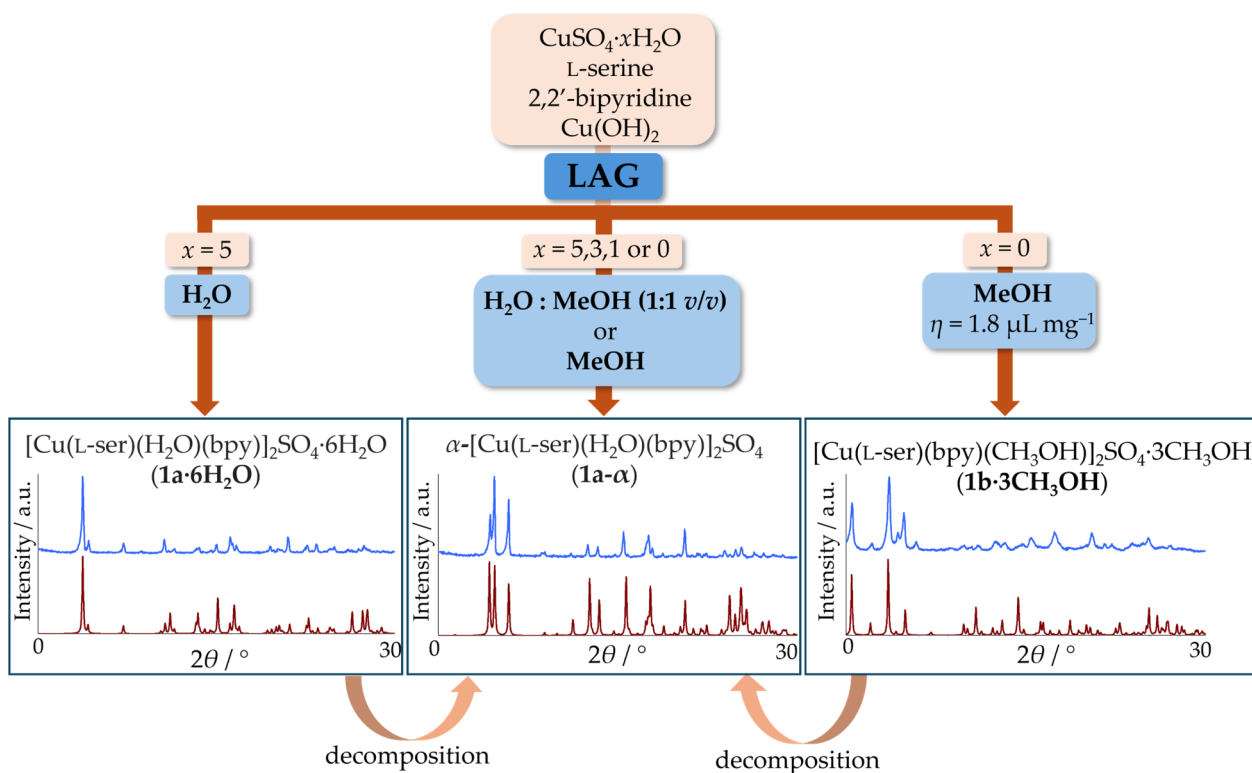


**Figure 2.** Schematic diagram of mechanochemical syntheses with powder X-ray diffraction patterns of the products of mechanochemical reactions. Blue PXRD patterns were experimentally measured, and red ones were calculated from crystal structure.

Mechanochemical synthesis was shown to be a better method for the preparation of **1a- $\alpha$** . Four reactants in the solid state were chosen, so no byproducts were formed in the case of a complete reaction. We used anhydrous or different hydrates of copper(II) sulfate (monohydrate, trihydrate, pentahydrate), copper(II) hydroxide, 2,2'-bipyridine, and L-serine, and in most cases water or methanol (which were in some reactions also reactants). Typically, those reactants yielded one pure product, and in some cases, mixtures of known or unknown phases. All products were analysed by PXRD and compared with powder diffraction patterns calculated from crystal structures of **1a·6H<sub>2</sub>O**, **1a- $\alpha$** , and **1b·3CH<sub>3</sub>OH**. In most synthetic conditions we investigated, **1a- $\alpha$**  was formed in pure form in a short time (15 min of milling). We prepared **1a·6H<sub>2</sub>O** (Table S1, Figures S1–S3) and **1b·3CH<sub>3</sub>OH** (Table S3, Figure S19) by mechanochemical synthesis. These two compounds form unstable crystals, so they started decomposing immediately after opening the jar (Figures S1 and S19). We showed that the syntheses are highly dependent on water content. If more water ( $\eta = 0.1$  or  $0.2 \mu\text{L mg}^{-1}$ ) is used for LAG, **1a·6H<sub>2</sub>O** is formed, while at lower water content (neat grinding or liquid-assisted grinding, LAG, with methanol/water mixture or pure methanol), **1a- $\alpha$**  is the product of the reaction. In some cases, a small amount of unidentified phase was formed along with **1a- $\alpha$**  (Tables S1–S3). If anhydrous copper(II) sulfate was used in LAG with methanol, **1a- $\alpha$**  or **1b·3CH<sub>3</sub>OH** was formed (Figures 2 and S14–S19). For the synthesis of **1b·3CH<sub>3</sub>OH**, the  $\eta$ -parameter, which is widely used for systematic approaches to mechanochemical synthesis [15,58], was  $1.8 \mu\text{L mol}^{-1}$ . Methanol had to be in surplus to prepare **1b·3CH<sub>3</sub>OH**. Such a large amount of solvent relative to the mass of solid reactants is not usually considered a mechanochemical reaction (limit is typically set to  $\eta = 1.0 \mu\text{L mg}^{-1}$ , [18,58]); however, methanol was also one of the reactants, entering the crystal structure. Along with the  $\eta$ -parameter, in the synthesis of solvates such as this, one should also consider the amount of solvent that will be absorbed into the crystal structure of the products. In our case, such a large surplus of methanol was needed probably because of the presence of water in the reaction mixture, the air, and the milling jar, as well as forming as a product of the reaction; thus, more methanol was needed for successful formation of **1b·3CH<sub>3</sub>OH**.

### 3.2. Solvent Exchange in Solid State

#### 3.2.1. Transformations **1a·6H<sub>2</sub>O** $\rightleftharpoons$ **1a- $\alpha$** , **1a·6H<sub>2</sub>O** $\rightarrow$ **1a- $\beta$** and **1a- $\alpha$** $\rightarrow$ **1a- $\beta$**

The formation of different solvates enables the potential application of these compounds as sensors or adsorbents. We explored the stability of **1a·6H<sub>2</sub>O** and **1a- $\alpha$** , and the conversions **1a·6H<sub>2</sub>O**  $\rightleftharpoons$  **1a- $\alpha$** , **1a·6H<sub>2</sub>O**  $\rightarrow$  **1a- $\beta$** , and **1a- $\alpha$**   $\rightarrow$  **1a- $\beta$** , in solid state. If **1a·6H<sub>2</sub>O** is placed in atmospheres of different relative humidities (*RH*), it readily converts into **1a- $\alpha$**  (Figures 3 and S20). The rate of conversion is dependent on relative humidity, where at *RH*  $\approx$  0% it is completely converted into **1a- $\alpha$**  after a few minutes. Conversion **1a·6H<sub>2</sub>O**  $\rightarrow$  **1a- $\alpha$**  proceeds through an unknown intermediate phase, **IP1**, possibly a hydrate with lower water content, which was present even at *RH* = 9% after 4 weeks. **1a·6H<sub>2</sub>O** completely decomposes into the intermediate phase and **1a- $\alpha$**  at *RH* < 65%. **1a- $\alpha$** , on the other hand, is stable at low values of *RH*, even at *RH*  $\approx$  0% (Figures 3 and S21). At *RH* = 65%, an intermediate phase **IP1** (the same phase as in **1a·6H<sub>2</sub>O**  $\rightarrow$  **1a- $\alpha$**  conversion) starts to form. At *RH* > 95%, **1a·6H<sub>2</sub>O** starts to form, but **1a- $\alpha$**   $\rightarrow$  **1a·6H<sub>2</sub>O** conversion was not complete after 4 weeks.

We also explored the stability of **1a- $\alpha$**  and **1a·6H<sub>2</sub>O** in an atmosphere of methanol vapours. Both compounds were placed in a methanol vapour atmosphere and monitored by ex situ PXRD measurements. **1a·6H<sub>2</sub>O** transforms partly into **1a- $\alpha$** , but in both experiments, diffraction maxima of **1a- $\beta$**  were observed after 4 weeks (Figure 4). These results confirmed that the presence of methanol is needed for the formation of **1a- $\beta$** , as was observed in solution-based synthesis experiments.



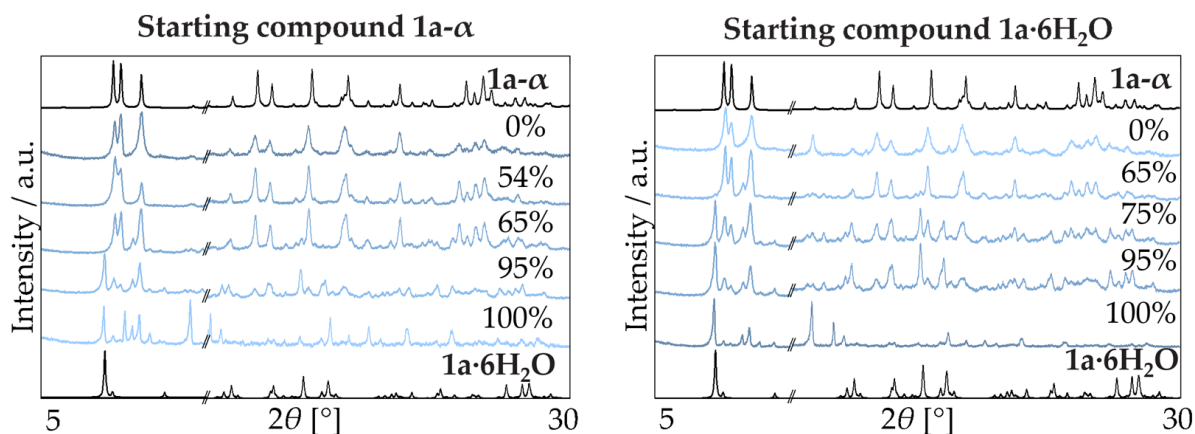


**Figure 3.** PXRD diffraction patterns of **1a-α** (left) and **1a·6H<sub>2</sub>O** (right) after aging for 4 weeks in atmospheres of different relative humidities. Diffraction patterns separated by a broken line are not on the same intensity scale. Blue PXRD patterns were experimentally measured, and black ones were calculated from crystal structure.

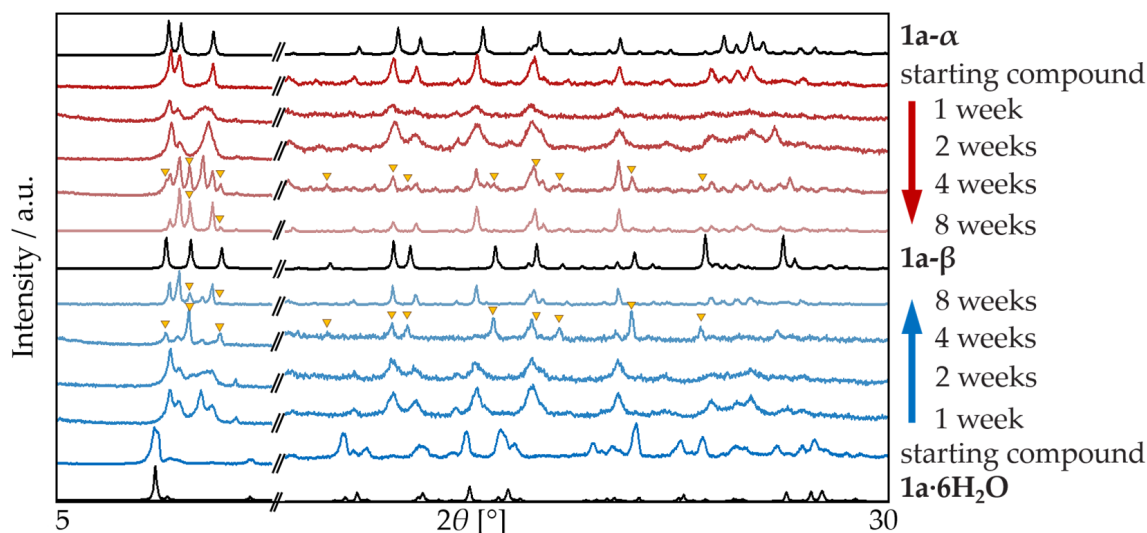


**Figure 4.** PXRD patterns of **1a-α** (red) and **1a·6H<sub>2</sub>O** (blue) after aging in an atmosphere of methanol vapours. PXRD patterns calculated from the single-crystal data are shown in black. Yellow triangles show diffraction peaks characterized as **1a-β**. Diffraction patterns separated by a broken line are not on the same intensity scale. Single-crystal data for all compounds were measured at 100 K, so shifts of some diffraction maxima are possible.

### 3.2.2. Transformation **1b·3CH<sub>3</sub>OH** → **1a-α**

We obtained **1b·3CH<sub>3</sub>OH** mechanochemically with a large amount of methanol, with  $\eta = 1.8 \mu\text{L mol}^{-1}$ . Immediately upon opening the jar, **1b·3CH<sub>3</sub>OH** decomposed to **1a-α** as observed by PXRD. After 2 min, only **1a-α** was present in the solid sample (Figure S19).

### 3.3. Thermogravimetric Analysis (TGA) and Infrared Spectroscopy (IR)

Only **1a-α** was analysed using thermogravimetric analysis and infrared spectroscopy. **1a·6H<sub>2</sub>O** and **1b·3CH<sub>3</sub>OH** decompose too fast to be analysed properly by these methods, and **1a-β** was not obtained in pure form. **1a-α** loses its coordinated water molecule at approximately 90 °C (exp. 4.2% of mass loss, theor. 4.6%) in a wide step that partially overlaps with the start of the decomposition of organic ligands (at 170 °C). Most of the components decompose up to 480 °C (residue is 21.6%), but there is another small decomposition step at 670–720 °C with a weight loss of 1.0% (Figure S22). After 720 °C, the residue is copper(II) oxide (exp. 19.9%, theor. 20.4%).

The infrared spectrum of **1a- $\alpha$**  revealed extensive hydrogen bonding with several broad bands (Figure S23). Bands at 3433–3037  $\text{cm}^{-1}$  correspond to stretching vibrations of  $\nu(\text{O-H})$  and  $\nu(\text{N-H})$ . Aliphatic C–H vibrations are at 2941 and 2878  $\text{cm}^{-1}$ . The strong band at 1626  $\text{cm}^{-1}$  was assigned to the stretching of the delocalized carboxylate group of the L-serinato ligand, and that at 1601  $\text{cm}^{-1}$ , to a combination of the stretching of the carboxylate group and the bending of amino-group [59]. The bands at 417 and 410  $\text{cm}^{-1}$  correspond to the stretching of Cu–O and/or Cu–N bonds.

### 3.4. Crystal Structures

All four compounds are composed of complex cations  $[\text{Cu}(\text{L-ser})(\text{bpy})(\text{L})]^+$  ( $\text{L} = \text{H}_2\text{O}$  or  $\text{CH}_3\text{OH}$ ) with square-pyramidal geometry. L-Ser and bpy are bonded to copper in a chelate ring in an equatorial plane and water or methanol molecule is apically coordinated. Because of the Jahn–Teller effect, apical Cu–O bonds are elongated with distances 2.205(8)–2.347(4) Å (Table S5). Complex cations  $[\text{Cu}(\text{L-ser})(\text{bpy})(\text{L})]^+$  ( $\text{L} = \text{H}_2\text{O}$  or  $\text{CH}_3\text{OH}$ ) are stacked through  $\pi$ -interactions in 1D infinite pillars (Figure 5). Pillars are further interconnected through  $\text{O}_{\text{water/methanol}}-\text{H}\cdots\text{O}_{\text{carboxylate}}$  and  $\text{N}-\text{H}\cdots\text{O}_{\text{hydroxyl}}$  hydrogen bonds, forming a 3D supramolecular framework (Figure S26, Table S6).

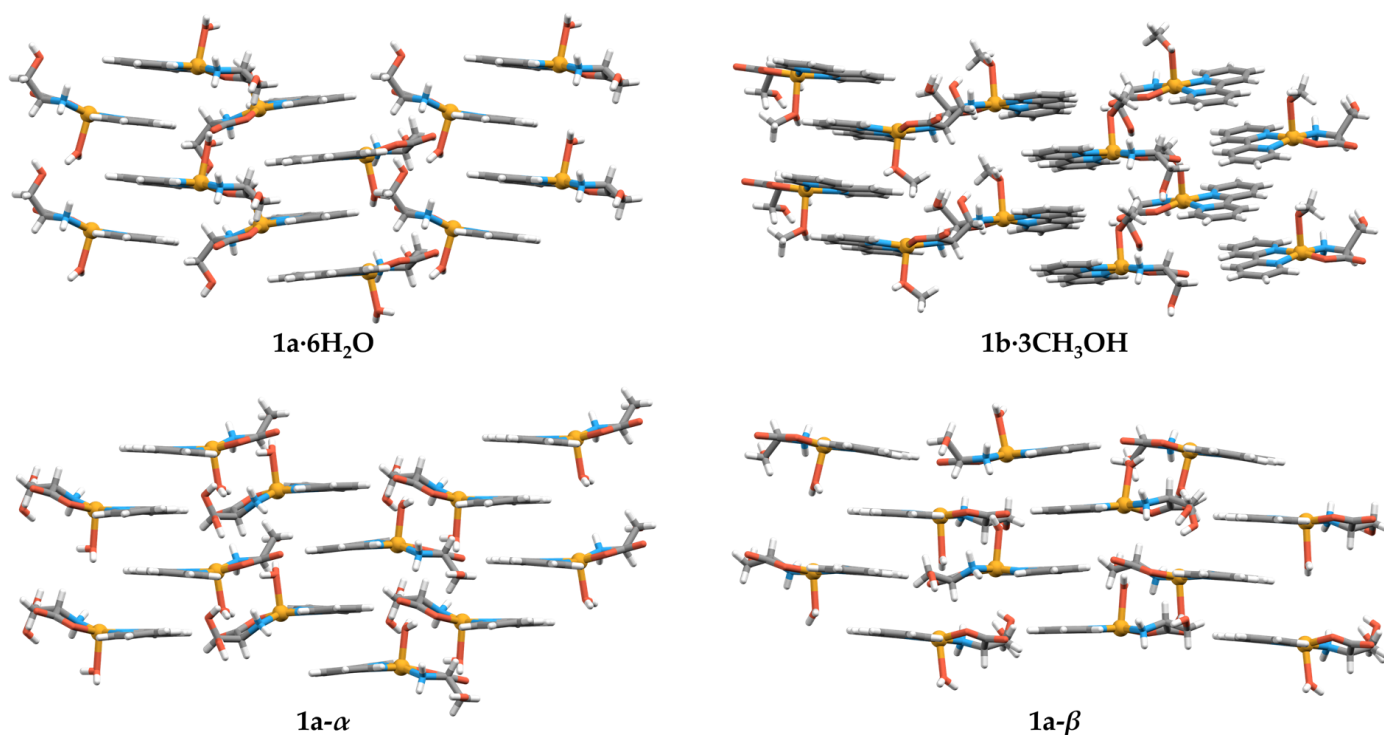
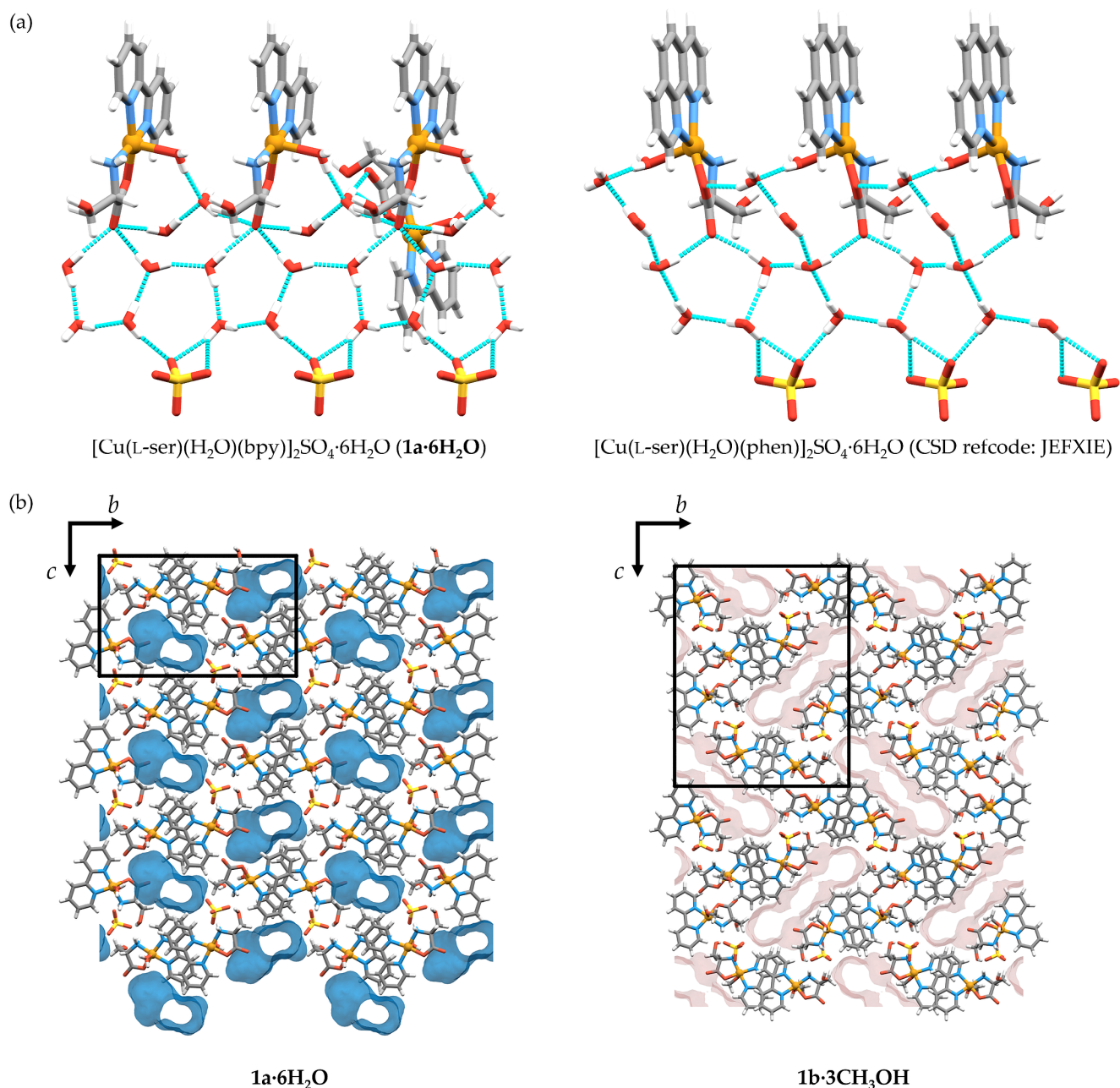


Figure 5.  $\pi$ -stacked pillars in **1a·6H<sub>2</sub>O**, **1a- $\alpha$** , **1a- $\beta$** , and **1b·3CH<sub>3</sub>OH**.

All compounds contain numerous donors (water or methanol molecules, amino and hydroxyl groups) and acceptors (sulfate ions, water or methanol molecules, carboxylate and hydroxyl groups) of hydrogen bonds forming complex frameworks. **1a·6H<sub>2</sub>O** forms a 3D framework of hydrogen bonds (Figure S26), where crystallization water molecules connect neighbouring  $\pi$ -stacked pillars of complex cations and sulfate ions. Four crystallization water molecules are propagated by 5-membered hydrogen-bonded rings along the  $a$ -axis involving  $\text{O}_{\text{water}}-\text{H}\cdots\text{O}_{\text{carboxylate}}$ ,  $\text{O}_{\text{water}}-\text{H}\cdots\text{O}_{\text{sulfate}}$  and  $\text{O}_{\text{water}}-\text{H}\cdots\text{O}_{\text{water}}$  hydrogen bonds (Table S6) and forming infinite 1D channels (Figure 6a,b). A similar hydrogen bonding pattern is found in  $[\text{Cu}(\text{L-ser})(\text{H}_2\text{O})(\text{phen})]_2\text{SO}_4\cdot 6\text{H}_2\text{O}$  (phen = 1,10-phenanthroline; CSD refcode: JEFXIE [28], Figure 6a). Nevertheless, **1a·6H<sub>2</sub>O** is unstable outside of solution decomposing to **1a- $\alpha$** , while JEFXIE is stable for months, suggesting that other structural features also significantly influence the stability of crystal structure. Crystallization water

molecules form 1D channels and occupy 15.9% of the unit cell volume. Similarly, crystallization methanol molecules in **1b**·3CH<sub>3</sub>OH form 1D channels occupying 20.9% of the unit cell volume. In both cases, the crystal structures are unstable and lose solvent molecules. **1b**·3CH<sub>3</sub>OH decomposes more quickly because of the weaker interactions of methanol molecules compared with the water molecules in **1a**·6H<sub>2</sub>O.



**Figure 6.** (a) Comparison of propagation of water molecules through hydrogen bonding along the *a*-axis in **1a**·6H<sub>2</sub>O and [Cu(L-ser)(H<sub>2</sub>O)(phen)]<sub>2</sub>SO<sub>4</sub>·6H<sub>2</sub>O; (b) 1D channels of solvent molecules (water in blue, methanol in pink) in **1a**·6H<sub>2</sub>O and **1b**·3CH<sub>3</sub>OH.

The two polymorphs **1a- $\alpha$**  and **1a- $\beta$**  have similar structural features and intermolecular interactions. In both structures, complex cations form 2D layers through  $\pi$ -interactions and O<sub>water</sub>-H $\cdots$ O<sub>carboxylate</sub> hydrogen bonds. Sulfate ions are located between layers and act as a bridge between them through O<sub>water</sub>-H $\cdots$ O<sub>sulfate</sub>, O<sub>hydroxyl</sub>-H $\cdots$ O<sub>sulfate</sub>, and N-H $\cdots$ O<sub>sulfate</sub> hydrogen bonds (Table S6). Both polymorphs form 2D hydrogen bond

networks (Figure 7). In **1a- $\alpha$** , three out of four symmetrically independent complex cations form N–H $\cdots$ O<sub>hydroxyl</sub> hydrogen bonds between those layers, while in **1a- $\beta$** , only one complex cation forms such a bond. Another significant difference between **1a- $\alpha$**  and **1a- $\beta$**  is in the relative orientation of 2D layers. In **1a- $\alpha$** , layers are tilted to each other by approximately 26.5°, while in **1a- $\beta$** , they are coplanar (Figure 7).

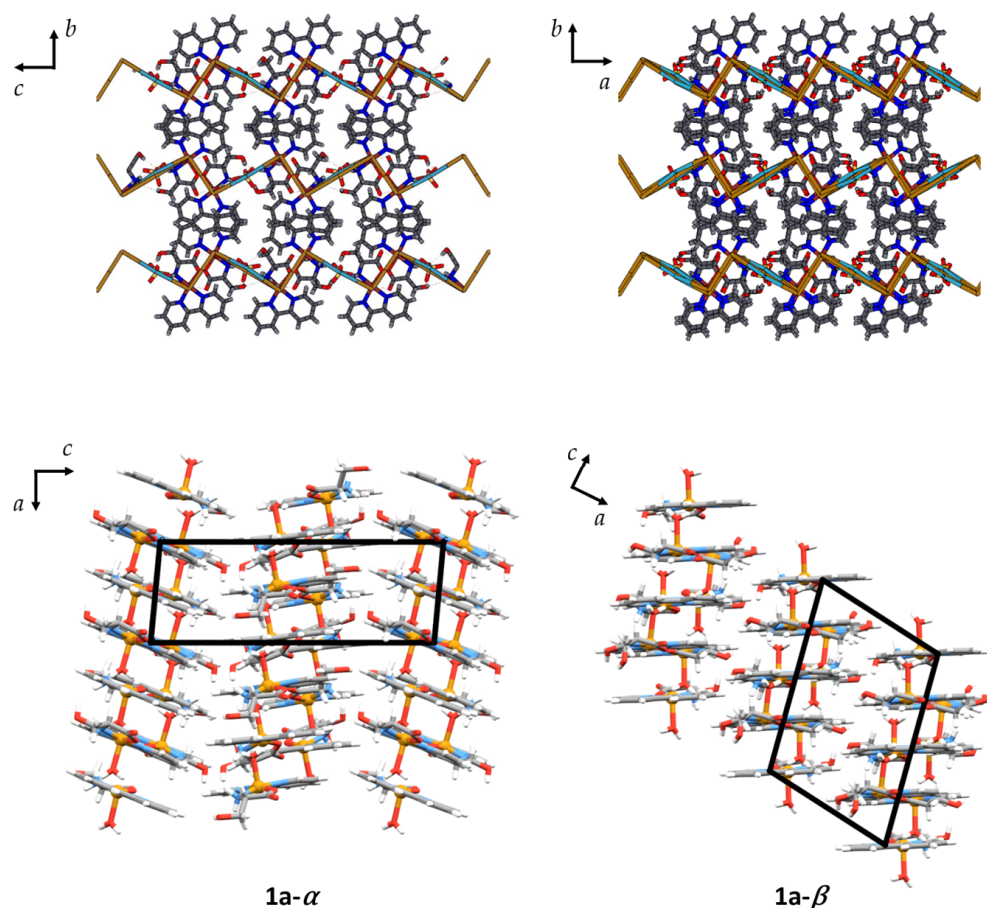


**Figure 7.** Differences in the structures of **1a- $\alpha$**  and **1a- $\beta$** .  $\pi$ -stacked layers of complex cations and a simplified view of propagation of hydrogen bonds are shown in the top pictures. Brown lines represent hydrogen bonds formed by complex cations, and light blue lines represent hydrogen bonds formed by sulfate ions. The difference in the relative angles of the  $\pi$ -stacked layers is shown in the bottom pictures.

### 3.4.1. Hirshfeld Surface Analysis

Hirshfeld surface analysis was performed for each symmetrically independent cation to better understand the differences in the intermolecular contacts in the structures of **1a- $\alpha$**  and **1a- $\beta$** . The differences in the distribution of interatomic contacts in the complex cations are very small. On average, the complex cations in **1a- $\alpha$**  contain slightly more O $\cdots$ H/H $\cdots$ O contacts (33.4% in **1a- $\alpha$** , 32.0% in **1a- $\beta$** ). **1a- $\beta$**  contains more C $\cdots$ O/O $\cdots$ C (1.1% in **1a- $\alpha$** , 2.1% in **1a- $\beta$** ) and H $\cdots$ H (38.8% in **1a- $\alpha$** , 39.9% in **1a- $\beta$** ) contacts (Figure 8). If we inspect the differences between each cation, we can see that cation 4 in **1a- $\alpha$**  has significantly more O $\cdots$ H/H $\cdots$ O (37.6%) and fewer H $\cdots$ H (35.5%) than other cations in **1a- $\alpha$**  (range of O $\cdots$ H/H $\cdots$ O contacts, 31.5–32.3%; range of H $\cdots$ H contacts, 39.6–40.2%) or **1a- $\beta$**  (range of O $\cdots$ H/H $\cdots$ O contacts, 30.8–33.1%; range of H $\cdots$ H contacts, 38.7–41.4%). The main reason for this difference is disordered serine residue, and both positions were taken into account for calculations. **1a- $\beta$**  also contains one complex cation with disordered serine residue, but the disordered residues are closer to each other and do not contribute to such a difference. In general, small deviations in interatomic contacts

suggested that polymorphs form similar types of intermolecular interactions and that the main difference between them is in the geometric features of crystal packing.

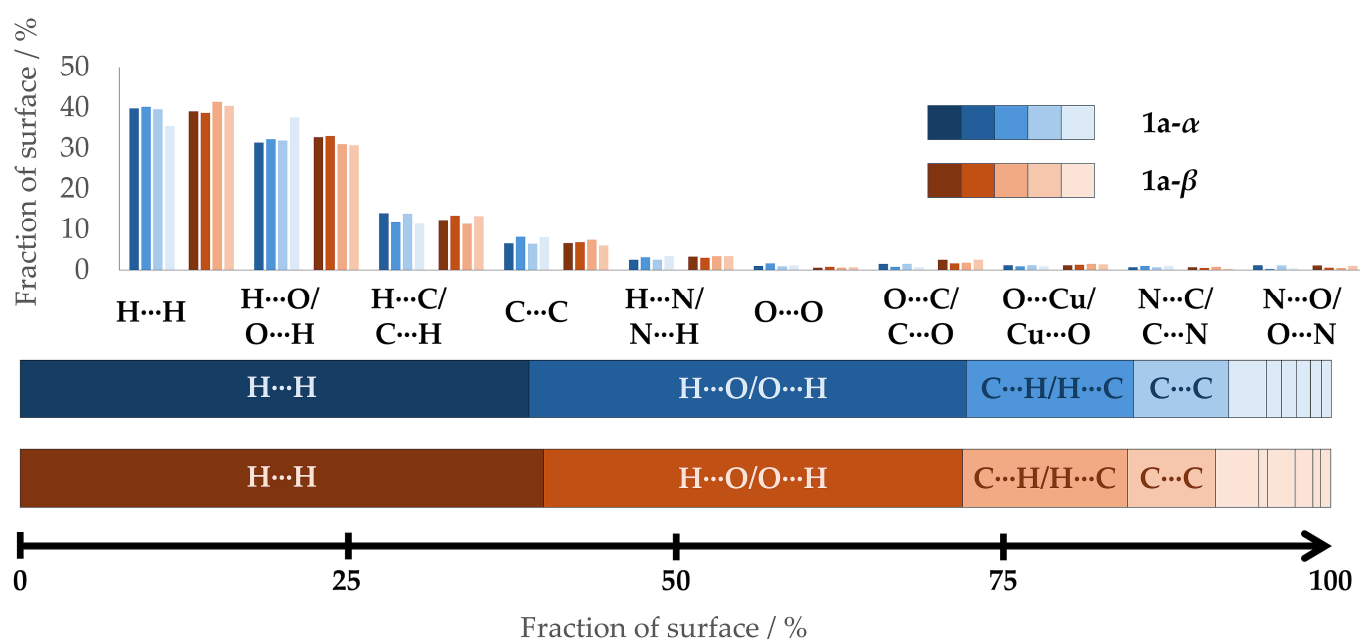


**Figure 8.** Distribution of interatomic contacts as a fraction of the Hirshfeld surface of each symmetrically independent cation (top graph) and average values for all cations (bottom lines) in **1a-α** and **1a-β**.

#### 3.4.2. Molecular Movements During $1\mathbf{a}\cdot 6\mathbf{H}_2\mathbf{O} \rightleftharpoons 1\mathbf{a}\text{-}\alpha$ and $1\mathbf{b}\cdot 3\mathbf{CH}_3\mathbf{OH} \rightarrow 1\mathbf{a}\text{-}\alpha$ Transformations in Solid State

During  $1\mathbf{a}\cdot 6\mathbf{H}_2\mathbf{O} \rightleftharpoons 1\mathbf{a}\text{-}\alpha$  in solid state, some molecular motions are involved in transformation. In the  $1\mathbf{a}\cdot 6\mathbf{H}_2\mathbf{O} \rightarrow 1\mathbf{a}\text{-}\alpha$  transition,  $1\mathbf{a}\cdot 6\mathbf{H}_2\mathbf{O}$  loses crystallization water molecules, and to fill the empty space, 1D  $\pi$ -stacked pillars rotate and move closer to each other, forming 2D layers between sulfate ions (Figure 9). The coordination of half of the complex cations also changes. In  $\pi$ -stacked pillars of  $1\mathbf{a}\cdot 6\mathbf{H}_2\mathbf{O}$ , apically coordinated water molecules alternate in an up–down fashion. This trend changes in **1a-α**, where all apically coordinated water molecules within the same pillar are oriented in the same direction, but the neighbouring pillars of the same 2D layers alternate in an up–down fashion. Possibly, a coordinated water molecule switches position from one copper atom to another as shown in Figure 9, since it is the closest water molecule to a copper atom.

During the  $1\mathbf{b}\cdot 3\mathbf{CH}_3\mathbf{OH} \rightarrow 1\mathbf{a}\text{-}\alpha$  transition,  $1\mathbf{b}\cdot 3\mathbf{CH}_3\mathbf{OH}$  loses methanol molecules and absorbs water from the air, which coordinates to copper atoms. After crystallization, methanol molecules are desorbed from  $1\mathbf{b}\cdot 3\mathbf{CH}_3\mathbf{OH}$ ; 1D  $\pi$ -stacked pillars are involved in similar movements as in the  $1\mathbf{a}\cdot 6\mathbf{H}_2\mathbf{O} \rightarrow 1\mathbf{a}\text{-}\alpha$  transition (Figure 10).

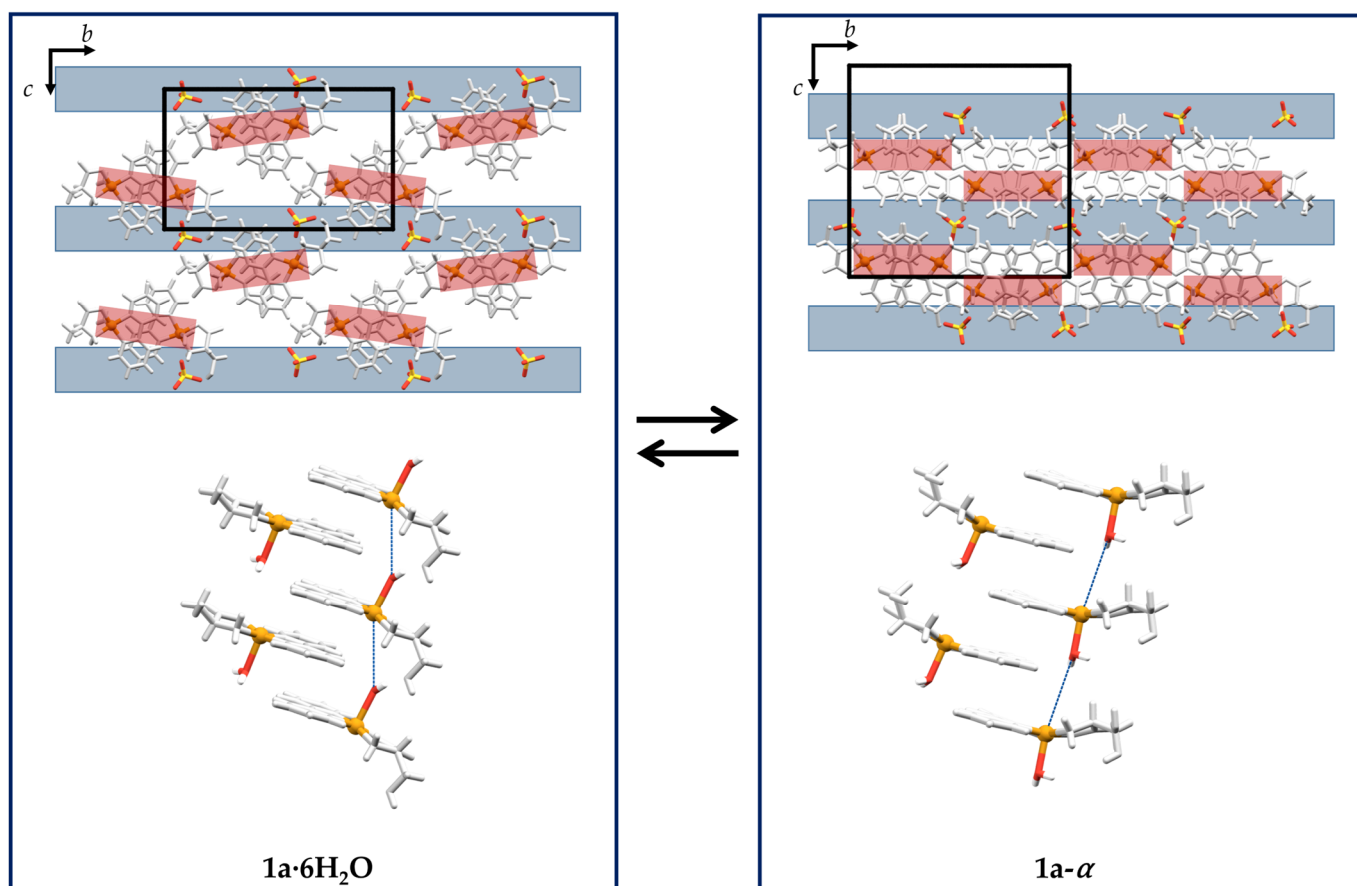


**Figure 9.** Movements of 1D  $\pi$ -stacked pillars and sulfate ions (**top**) and the change in the coordination of water molecules (**bottom**) during  $1\mathbf{a}\cdot 6\mathbf{H}_2\mathbf{O} \rightleftharpoons 1\mathbf{a}\text{-}\alpha$  transformation. Possible movements of water molecules are shown with blue dashed lines.

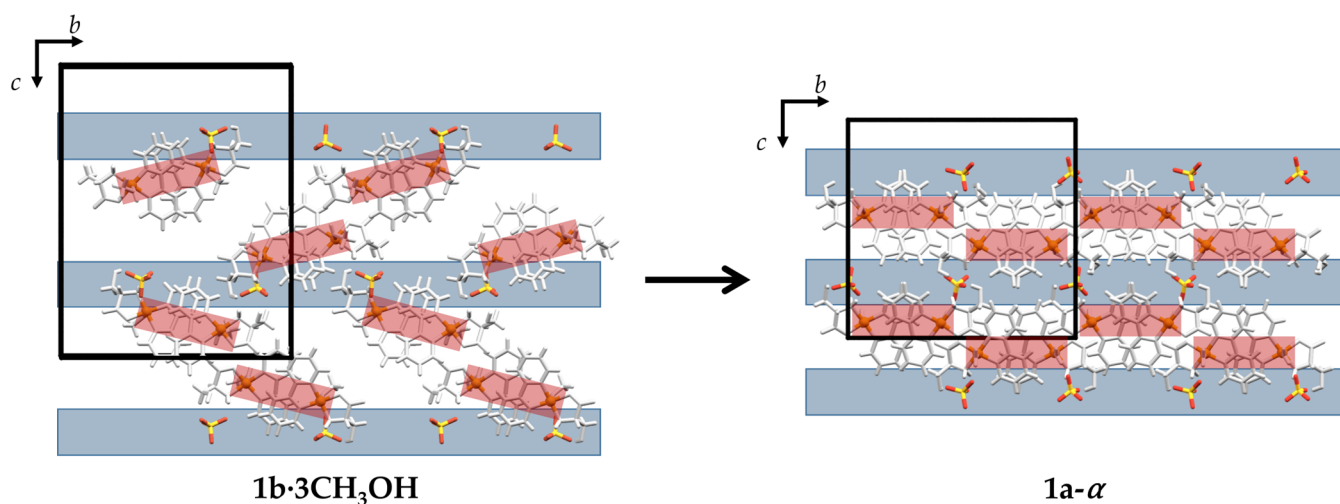


**Figure 10.** Movements of 1D  $\pi$ -stacked pillars and sulfate ions during the  $1\mathbf{b}\cdot 3\mathbf{CH}_3\mathbf{OH} \rightarrow 1\mathbf{a}\text{-}\alpha$  transition.

### 3.5. Proliferation Assays

The antiproliferative activities of **1a-α** were measured on three human cell lines derived from three cancer types, H460 (lung carcinoma), MCF-7 (breast carcinoma), and HCT116 (colon carcinoma), using the MTT test. **1a-α** had moderate activity towards all three tested cell lines.  $IC_{50}$  values were comparable to and slightly higher than those of the known antitumour agents

etoposide, 5-fluorouracil, and  $[\text{Cu}(\text{L-ser})(\text{H}_2\text{O})(\text{phen})]_2\text{SO}_4 \cdot 6\text{H}_2\text{O}$  [28,56,57] (Table 1). These results give us valuable information for the design of compounds with higher antiproliferative activities. These data support results in the literature that the heterocyclic base is the key factor influencing the antiproliferative activity of ternary coordination compounds [12].

**Table 1.**  $IC_{50}$  values of **1a- $\alpha$**  compared with  $[\text{Cu}(\text{L-ser})(\text{H}_2\text{O})(\text{phen})]_2\text{SO}_4 \cdot 6\text{H}_2\text{O}$ , etoposide, and 5-fluorouracil (in  $\mu\text{M}$ ).

Compound	$IC_{50}^a/10^{-6} \text{ mol dm}^{-3}$		
	Cell Lines		
	HCT116	MCF-7	H 460
<b>1a-<math>\alpha</math></b>	$10 \pm 1$	$18 \pm 3$	$14 \pm 2$
$[\text{Cu}(\text{L-ser})(\text{H}_2\text{O})(\text{phen})]_2\text{SO}_4 \cdot 6\text{H}_2\text{O}$	- <sup>b</sup>	$2 \pm 0.08$ <sup>c</sup>	$2 \pm 0.2$ <sup>c</sup>
etoposide	$5 \pm 2$ <sup>d,e</sup>	$1 \pm 0.7$ <sup>d,e</sup>	$0.1 \pm 0.04$ <sup>d,e</sup>
5-fluorouracil	$4 \pm 1$ <sup>e</sup>	$14 \pm 0.3$ <sup>e</sup>	$3 \pm 0.3$ <sup>e</sup>

<sup>a</sup>  $IC_{50}$ —the concentration that causes 50% growth inhibition; <sup>b</sup> not measured; <sup>c</sup> [28]; <sup>d</sup> [57]; <sup>e</sup> [56].

#### 4. Conclusions

We successfully prepared four new ternary coordination compounds of copper(II), L-serine, and 2,2'-bipyridine by solution-based and mechanochemical syntheses. **1a·6H<sub>2</sub>O** and **1b·3CH<sub>3</sub>OH** are unstable outside of solution because of their large fractions of solvent molecules (15.9% and 20.9%, respectively) and crystal packing influence. Two polymorphs of  $[\text{Cu}(\text{L-ser})(\text{bpy})(\text{H}_2\text{O})]_2\text{SO}_4$  were crystallized, **1a- $\alpha$**  and **1a- $\beta$** . It was shown that the presence of water hinders the formation of **1a- $\beta$**  and promotes the crystallization of **1a- $\alpha$** , while methanol can be used for partial transformations **1a·6H<sub>2</sub>O**  $\rightarrow$  **1a- $\beta$**  and **1a- $\alpha$**   $\rightarrow$  **1a- $\beta$**  in the solid state. In mechanochemical synthesis, different amounts of water and methanol direct the formation of either **1a·6H<sub>2</sub>O** or **1a- $\alpha$**  at high water content, or either **1a- $\alpha$**  or **1b·3CH<sub>3</sub>OH** at low water and high methanol content. As shown here and in our previous research, in similar systems, it is advisable to perform fine-tuned screening of solvents to explore the solvatomorphic behaviour of compounds. During the **1a·6H<sub>2</sub>O**  $\rightarrow$  **1a- $\alpha$**  transition, cooperative movements of atoms occur. Crystallization water molecules desorb from the crystal, 1D  $\pi$ -stacked pillars move closer to each other, and the position of the coordinated water molecule is switched in half of the complex cations. Similar movements occur in **1b·3CH<sub>3</sub>OH**  $\rightarrow$  **1a- $\alpha$**  decomposition, where crystals spontaneously absorb water from the air to form **1a- $\alpha$** . Furthermore, **1a- $\alpha$**  can be considered as an activated form of porous compounds, with the ability to adsorb water and potentially methanol molecules. We showed that many supramolecular synthons are preserved in all four structures, which is useful for further design of similar compounds and aimed tuning of desired properties. These compounds show potential as sensors or adsorbers and as model compounds for more complex coordination systems. Moderate antiproliferative activity was shown **1a- $\alpha$**  towards three cell lines, H460 (lung carcinoma), MCF-7 (breast carcinoma), and HCT116.

**Supplementary Materials:** The following supporting information can be downloaded at: <https://www.mdpi.com/article/10.3390/cryst14110986/s1>, Figure S1: Experimental PXRD pattern (blue) of the products of synthesis no. 1 from Table S1 compared with calculated PXRD patterns from the crystal structures of **1a- $\alpha$**  and **1a·6H<sub>2</sub>O** (red); Figure S2: Experimental PXRD pattern (blue) of the products of synthesis no. 2 from Table S1 compared with calculated PXRD patterns from the crystal structure of **1a- $\alpha$**  (red); Figure S3: Experimental PXRD pattern (blue) of the products of synthesis no. 3 from Table S1 compared with calculated PXRD patterns from the crystal structure of **1a- $\alpha$**  (red); Figure S4: Experimental PXRD pattern (blue) of the products of synthesis no. 4 from Table S1 compared with calculated PXRD patterns from the crystal structure of **1a- $\alpha$**  (red); Figure S5: Experimental PXRD pattern (blue) of the products of synthesis no. 5 from Table S1 compared with calculated PXRD patterns from the crystal structure of **1a- $\alpha$**  (red); Figure S6: Experimental PXRD pattern (blue) of the products of synthesis no. 6 from Table S1 compared with calculated PXRD patterns from the crystal structure of **1a- $\alpha$**  (red); Figure S7: Experimental PXRD pattern (blue) of

the products of synthesis no. 7 from Table S1 compared with calculated PXRD patterns from the crystal structure of **1a- $\alpha$**  (red); Figure S8: Experimental PXRD pattern (blue) of the products of synthesis no. 8 from Table S2 compared with calculated PXRD patterns from the crystal structure of **1a- $\alpha$**  (red); Figure S9: Experimental PXRD pattern (blue) of the products of synthesis no. 9 from Table S2 compared with calculated PXRD patterns from the crystal structure of **1a- $\alpha$**  (red); Figure S10: Experimental PXRD pattern (blue) of the products of synthesis no. 10 from Table S2 compared with calculated PXRD patterns from the crystal structures of reactants (red); Figure S11: Experimental PXRD pattern (blue) of the products of synthesis no. 11 from Table S2 compared with calculated PXRD patterns from the crystal structure of **1a- $\alpha$**  (red); Figure S12: Experimental PXRD pattern (blue) of the products of synthesis no. 12 from Table S2 compared with calculated PXRD patterns from the crystal structure of **1a- $\alpha$**  (red); Figure S13: Experimental PXRD pattern (blue) of the products of synthesis no. 13 from Table S2 compared with calculated PXRD patterns from the crystal structures of reactants (red); Figure S14: Experimental PXRD pattern (blue) of the products of synthesis no. 14 from Table S3 compared with calculated PXRD patterns from the crystal structures of reactants (red); Figure S15: Experimental PXRD pattern (blue) of the products of synthesis no. 15 from Table S3 compared with calculated PXRD patterns from the crystal structure of **1a- $\alpha$**  (red); Figure S16: Experimental PXRD pattern (blue) of the products of synthesis no. 16 from Table S3 compared with calculated PXRD patterns from the crystal structure of **1a- $\alpha$**  (red); Figure S17: Experimental PXRD pattern (blue) of the products of synthesis no. 17 from Table S3 compared with calculated PXRD patterns from the crystal structure of **1a- $\alpha$**  (red); Figure S18: Experimental PXRD pattern (blue) of the products of synthesis no. 18 from Table S3 compared with calculated PXRD patterns from the crystal structure of **1a- $\alpha$**  (red); Figure S19: Experimental PXRD pattern of the products of synthesis no. 19 from Table S3 measured immediately upon opening the jar (blue) and after 2 min of standing in the air (light blue) compared with calculated PXRD patterns from the crystal structures of **1a- $\alpha$**  and **1b·3CH<sub>3</sub>OH** (red); Figure S20: Experimental PXRD patterns of **1a·6H<sub>2</sub>O** after aging 4 weeks (blue) in a humidity- and temperature-controlled chamber compared with calculated PXRD patterns from the crystal structures of **1a- $\alpha$**  and **1a·6H<sub>2</sub>O** (black); Figure S21: Experimental PXRD patterns of **1a- $\alpha$**  after aging 4 weeks (blue) in a humidity- and temperature-controlled chamber compared with calculated PXRD patterns from the crystal structures of **1a- $\alpha$**  and **1a·6H<sub>2</sub>O** (black); Figure S22: TGA curve of **1a- $\alpha$** ; Figure S23: IR(ATR) spectrum of **1a- $\alpha$** ; Figure S24: ORTEP plot of the asymmetric unit of **1a- $\alpha$**  and **1a- $\beta$**  with the atom labelling scheme in the copper coordination sphere. Crystallization water molecules and sulfate anion were omitted for clarity. Displacement ellipsoids were calculated at the 50% probability level; Figure S25: ORTEP plot of the asymmetric unit of **1a·6H<sub>2</sub>O** and **1b·3CH<sub>3</sub>OH** with the atom labelling scheme in the copper coordination sphere. Crystallization water/methanol molecules and sulfate anion were omitted for clarity. Displacement ellipsoids were calculated at the 50% probability level; Figure S26: Simplified hydrogen bond frameworks. Brown lines represent hydrogen bonds formed by complex cations [Cu(L-ser)(L)(bpy)]<sup>+</sup> (L = H<sub>2</sub>O or CH<sub>3</sub>OH); light blue lines, hydrogen bonds formed by sulfate ions; dark blue lines, hydrogen bonds formed by crystallization water molecules in **1a·6H<sub>2</sub>O**; and purple lines, hydrogen bonds formed by crystallization methanol molecules in **1b·3CH<sub>3</sub>OH**. Atoms are shown in the pictures on the left, while in the pictures in the middle and on the right, they are omitted for clarity; Figure S27: Concentration–response profiles for **1a- $\alpha$**  tested in vitro on HCT116, MCF-7, and H 460 cell lines; Table S1: Mechanochemical synthetic conditions and the amounts of reactants and solvents used for the reactions with copper(II) sulfate pentahydrate; Table S2: Mechanochemical synthetic conditions and the amounts of reactants and solvents used for the reactions with copper(II) sulfate trihydrate and monohydrate; Table S3: Mechanochemical synthetic conditions and the amounts of reactants and solvents used for the reactions with anhydrous copper(II) sulfate; Table S4: Crystallographic data for compounds **1a- $\alpha$** , **1a- $\beta$** , **1a·6H<sub>2</sub>O**, and **1b·3CH<sub>3</sub>OH**; Table S5: Distances (Å) within the polyhedra of copper coordination spheres in the crystal structures of **1a- $\alpha$** , **1a- $\beta$** , **1a·6H<sub>2</sub>O**, and **1b·3CH<sub>3</sub>OH**; Table S6: Selected hydrogen bonds in **1a- $\alpha$** , **1a- $\beta$** , **1a·6H<sub>2</sub>O**, and **1b·3CH<sub>3</sub>OH**.

**Author Contributions:** Conceptualization, D.V. and B.P.; methodology, D.V. and B.P.; validation, D.V. and B.P.; formal analysis, D.V. and B.P.; investigation, D.V., M.P. and B.P.; resources, B.P.; data curation, D.V., M.P. and B.P.; writing—original draft preparation, D.V., M.P. and B.P.; visualization, D.V., M.P. and B.P.; supervision, B.P.; project administration, B.P.; funding acquisition, B.P. All authors have read and agreed to the published version of the manuscript.



**Funding:** This research was funded by the project CluK cofinanced by the Croatian Government and the European Regional Development Fund—Competitiveness and Cohesion Operational Programme (Grant KK.01.1.1.02.0016) and an institutional project financed by the University of Zagreb entitled *Synthesis and Structural Characterization of Organic and Complex Compounds; Protein Structure*.

**Data Availability Statement:** The original contributions presented in this study are included in the article/Supplementary Materials. Further inquiries can be directed to the corresponding author(s). CCDC 2393621-2393624 contain the supplementary crystallographic data for this paper. These data can be obtained free of charge via <https://www.ccdc.cam.ac.uk/structures/> (accessed on 23 October 2024) or from the CCDC, 12 Union Road, Cambridge CB2 1EZ, UK; Fax: +44 1223 336033; Email: de-posit@ccdc.cam.ac.uk.

**Acknowledgments:** We thank Nicola Demitri and Annie Heroux for their valuable support at Synchrotron Elettra in Trieste, and Marijeta Kralj and Lidija Uzelac from the Ruđer Bošković Institute for measuring the biological activity of compound **1a- $\alpha$** .

**Conflicts of Interest:** The authors declare no conflicts of interest.

## References

1. Patra, A.K.; Roy, S.; Chakravarty, A.R. Synthesis, Crystal Structures, DNA Binding and Cleavage Activity of L-Glutamine Copper(II) Complexes of Heterocyclic Bases. *Inorganica Chim. Acta* **2009**, *362*, 1591–1599. [CrossRef]
2. Chetana, P.R.; Rao, R.; Roy, M.; Patra, A.K. New Ternary Copper(II) Complexes of L-Alanine and Heterocyclic Bases: DNA Binding and Oxidative DNA Cleavage Activity. *Inorganica Chim. Acta* **2009**, *362*, 4692–4698. [CrossRef]
3. Ruiz-Azuara, L.; Bravo-Gomez, M.E. Copper Compounds in Cancer Chemotherapy. *Curr. Med. Chem.* **2010**, *17*, 3606–3615. [CrossRef]
4. García-Ramos, J.C.; Galindo-Murillo, R.; Tovar-Tovar, A.; Alonso-Saenz, A.L.; Gómez-Vidales, V.; Flores-Álamo, M.; Ortiz-Frade, L.; Cortes-Guzmán, F.; Moreno-Esparza, R.; Campero, A.; et al. The  $\pi$ -Back-Bonding Modulation and Its Impact in the Electronic Properties of  $\text{Cu}^{\text{II}}$  Antineoplastic Compounds: An Experimental and Theoretical Study. *Chem.—A Eur. J.* **2014**, *20*, 13730–13741. [CrossRef]
5. Patra, A.K.; Dhar, S.; Nethaji, M.; Chakravarty, A.R. Metal-Assisted Red Light-Induced DNA Cleavage by Ternary L-Methionine Copper(II) Complexes of Planar Heterocyclic Bases. *Dalton Trans.* **2005**, 896–902. [CrossRef]
6. Espinoza Guillén, A.; García Conde, D.; García Conde, F.; Fuentes Noriega, I.; Ruiz-Azuara, L. Casiopeina Parenteral Composition and Uses of the Same. Mexican Patent MX2017016444A, 17 June 2019.
7. Erxleben, A. Interactions of Copper Complexes with Nucleic Acids. *Coord. Chem. Rev.* **2018**, *360*, 92–121. [CrossRef]
8. Valencia-Cruz, A.I.; Uribe-Figueroa, L.I.; Galindo-Murillo, R.; Baca-López, K.; Gutiérrez, A.G.; Vázquez-Aguirre, A.; Ruiz-Azuara, L.; Hernández-Lemus, E.; Mejía, C. Whole Genome Gene Expression Analysis Reveals Casiopeina-Induced Apoptosis Pathways. *PLoS ONE* **2013**, *8*, e54664. [CrossRef]
9. Gutiérrez, A.G.; Vázquez-Aguirre, A.; García-Ramos, J.C.; Flores-Alamo, M.; Hernández-Lemus, E.; Ruiz-Azuara, L.; Mejía, C. Copper(II) Mixed Chelate Compounds Induce Apoptosis through Reactive Oxygen Species in Neuroblastoma Cell Line CHP-212. *J. Inorg. Biochem.* **2013**, *126*, 17–25. [CrossRef]
10. Becco, L.; García-Ramos, J.C.; Azuara, L.R.; Gambino, D.; Garat, B. Analysis of the DNA Interaction of Copper Compounds Belonging to the Casiopeinas<sup>®</sup> Antitumoral Series. *Biol. Trace Elem. Res.* **2014**, *161*, 210–215. [CrossRef]
11. Aguilar-Jiménez, Z.; Espinoza-Guillén, A.; Resendiz-Acevedo, K.; Fuentes-Noriega, I.; Mejía, C.; Ruiz-Azuara, L. The Importance of Being Casiopeina as Polypharmacological Profile (Mixed Chelate–Copper(II) Complexes and Their In Vitro and In Vivo Activities). *Inorganics* **2023**, *11*, 394. [CrossRef]
12. Bravo-Gómez, M.E.; García-Ramos, J.C.; Gracia-Mora, I.; Ruiz-Azuara, L. Antiproliferative Activity and QSAR Study of Copper(II) Mixed Chelate  $[\text{Cu}(\text{N}-\text{N})(\text{Acetylacetonato})]\text{NO}_3$  and  $[\text{Cu}(\text{N}-\text{N})(\text{Glycinato})]\text{NO}_3$  Complexes, (Casiopeinas<sup>®</sup>). *J. Inorg. Biochem.* **2009**, *103*, 299–309. [CrossRef]
13. Groom, C.R.; Bruno, I.J.; Lightfoot, M.P.; Ward, S.C. The Cambridge Structural Database. *Acta Crystallogr. B Struct. Sci. Cryst. Eng. Mater.* **2016**, *72*, 171–179. [CrossRef]
14. James, S.L.; Adams, C.J.; Bolm, C.; Braga, D.; Collier, P.; Friščić, T.; Grepioni, F.; Harris, K.D.M.; Hyett, G.; Jones, W.; et al. Mechanochemistry: Opportunities for New and Cleaner Synthesis. *Chem. Soc. Rev.* **2012**, *41*, 413–447. [CrossRef]
15. Friščić, T.; Childs, S.L.; Rizvi, S.A.A.; Jones, W. The Role of Solvent in Mechanochemical and Sonochemical Cocrystal Formation: A Solubility-Based Approach for Predicting Cocrystallisation Outcome. *CrystEngComm* **2009**, *11*, 418–426. [CrossRef]
16. Liu, Y.; Liu, F.; Li, S.; Liu, H.; Yan, K. Biasing the Formation of Solution-Unstable Intermediates in Coordination Self-Assembly by Mechanochemistry. *Chem.—A Eur. J.* **2023**, *29*, e202302563. [CrossRef]
17. Friščić, T.; Mottillo, C.; Titi, H.M. Mechanochemistry for Synthesis. *Angew. Chem. Int. Ed.* **2020**, *59*, 1030–1041. [CrossRef]
18. Do, J.-L.; Friščić, T. Mechanochemistry: A Force of Synthesis. *ACS Cent. Sci.* **2017**, *3*, 13–19. [CrossRef]
19. Užarević, K.; Štrukil, V.; Mottillo, C.; Julien, P.A.; Puškarić, A.; Friščić, T.; Halasz, I. Exploring the Effect of Temperature on a Mechanochemical Reaction by in Situ Synchrotron Powder X-Ray Diffraction. *Cryst. Growth Des.* **2016**, *16*, 2342–2347. [CrossRef]

20. Thebo, K.H.; Shad, H.A.; Thebo, A.A.; Raftery, J. Synthesis and Structural Characterization of Copper(II) Complex of 2,2'-Bipyridyl and L-Lysine. *Crystallogr. Rep.* **2014**, *59*, 1063–1067. [[CrossRef](#)]
21. Solans, X.; Ruíz-Ramírez, L.; Martínez, A.; Gasque, L.; Moreno-Esparza, R. Mixed Chelate Complexes. III. Structures of (L-Alaninato)(Aqua)(2,2'-Bipyridine)Copper(II) Nitrate Monohydrate and Aqua(2,2'-Bipyridine)(L-Tyrosinato)Copper(II) Chloride Trihydrate. *Acta Crystallogr. C* **1992**, *48*, 1785–1788. [[CrossRef](#)]
22. Zhang, W.C.; Lu, X. Long-Lived Photoluminescence and High Quantum Yield of Copper(II) Complexes with Novel Nanostructures. *RSC Adv.* **2015**, *5*, 101155–101161. [[CrossRef](#)]
23. Braban, M.; Haiduc, I.; Lönnecke, P. Catena-Poly[[[(2,2'-Bipyridyl)Copper(II)]- $\mu$ -L-Alaninato] Perchlorate Monohydrate]. *Acta Crystallogr. Sect. E Struct. Rep. Online* **2009**, *65*, m51. [[CrossRef](#)]
24. Subramanian, P.S.; Suresh, E.; Casella, L. Supramolecular Helical Architectures Dictated by Folded and Extended Conformations of the Amino Acid in Ternary CuII /Diamine/Racemic Amino Acid Complexes. *Eur. J. Inorg. Chem.* **2007**, *2007*, 1654–1660. [[CrossRef](#)]
25. Hua Zhou, X.; Yi Le, X.; Chen, S. Synthesis, Crystal Structure and Properties of a One-Dimensional L-Valinate Bridged Coordination Polymer: [Cu<sub>2</sub>(L-Val)<sub>2</sub>(Bpy)<sub>2</sub>]<sub>N</sub>·2nClO<sub>4</sub>·2nH<sub>2</sub>O. *J. Coord. Chem.* **2005**, *58*, 993–1001. [[CrossRef](#)]
26. Vušak, D.; Prugovečki, B.; Milić, D.; Marković, M.; Petković, I.; Kralj, M.; Matković-Čalogović, D. Synthesis and Crystal Structure of Solvated Complexes of Copper(II) with Serine and Phenanthroline and Their Solid-State-to-Solid-State Transformation into One Stable Solvate. *Cryst. Growth Des.* **2017**, *17*, 6049–6061. [[CrossRef](#)]
27. Perez Barrio, J.; Rebilly, J.; Carter, B.; Bradshaw, D.; Bacsá, J.; Ganin, A.Y.; Park, H.; Trewin, A.; Vaidhyanathan, R.; Cooper, A.I.; et al. Control of Porosity Geometry in Amino Acid Derived Nanoporous Materials. *Chem.—A Eur. J.* **2008**, *14*, 4521–4532. [[CrossRef](#)]
28. Zhang, Y.; Han, Y.; Luan, B.; Wang, L.; Yang, W.; Jiang, Y.; Ben, T.; He, Y.; Chen, B. Metal–Organic Framework with Space-Partition Pores by Fluorinated Anions for Benchmark C<sub>2</sub>H<sub>2</sub>/CO<sub>2</sub> Separation. *J. Am. Chem. Soc.* **2024**, *146*, 17220–17229. [[CrossRef](#)]
29. Jiang, Y.; Hu, Y.; Luan, B.; Wang, L.; Krishna, R.; Ni, H.; Hu, X.; Zhang, Y. Benchmark Single-Step Ethylene Purification from Ternary Mixtures by a Customized Fluorinated Anion-Embedded MOF. *Nat. Commun.* **2023**, *14*, 401. [[CrossRef](#)]
30. Alawadhi, A.H.; Chheda, S.; Strocio, G.D.; Rong, Z.; Kurandina, D.; Nguyen, H.L.; Rampal, N.; Zheng, Z.; Gagliardi, L.; Yaghi, O.M. Harvesting Water from Air with High-Capacity, Stable Furan-Based Metal–Organic Frameworks. *J. Am. Chem. Soc.* **2024**, *146*, 2160–2166. [[CrossRef](#)]
31. Song, W.; Zheng, Z.; Alawadhi, A.H.; Yaghi, O.M. MOF Water Harvester Produces Water from Death Valley Desert Air in Ambient Sunlight. *Nat. Water* **2023**, *1*, 626–634. [[CrossRef](#)]
32. Haldar, R.; Kumar, A.; Mandal, D.; Shanmugam, M. Deciphering the Anisotropic Energy Harvesting Responses of an above Room Temperature Molecular Ferroelectric Copper(II) Complex Single Crystal. *Mater. Horiz.* **2024**, *11*, 454–459. [[CrossRef](#)]
33. Yamada, M.; Shen, Z.; Miyake, M. Self-Assembly of Discotic Liquid Crystalline Molecule-Modified Gold Nanoparticles: Control of 1D and Hexagonal Ordering Induced by Solvent Polarity. *Chem. Commun.* **2006**, 2569–2571. [[CrossRef](#)]
34. Wang, W.; Su, K.; El-Sayed, E.-S.M.; Yang, M.; Yuan, D. Solvatomorphism Influence of Porous Organic Cage on C<sub>2</sub>H<sub>2</sub>/CO<sub>2</sub> Separation. *ACS Appl. Mater. Interfaces* **2021**, *13*, 24042–24050. [[CrossRef](#)] [[PubMed](#)]
35. Chimatahalli Shanthakumar, K.; Sridhara, P.G.; Rajabathar, J.R.; Al-Iohedan, H.A.; Lokanath, N.K.; Mlynahalli Krishnegowda, H. Unveiling a Novel Solvatomorphism of Anti-Inflammatory Flufenamic Acid: X-Ray Structure, Quantum Chemical, and In Silico Studies. *ACS Omega* **2024**, *9*, 20753–20772. [[CrossRef](#)]
36. Grell, T.; Barbero, M.; Pattarino, F.; Giovenzana, G.B.; Colombo, V. Solvatomorphism of Moxidectin. *Molecules* **2021**, *26*, 4869. [[CrossRef](#)]
37. Bhatia, A.; Chopra, S.; Nagpal, K.; Deb, P.K.; Tekade, M.; Tekade, R.K. Polymorphism and Its Implications in Pharmaceutical Product Development. In *Dosage Form Design Parameters*; Elsevier: Amsterdam, The Netherlands, 2018; pp. 31–65.
38. Ardila-Fierro, K.J.; Hernández, J.G. Intermediates in Mechanochemical Reactions. *Angew. Chem. Int. Ed.* **2024**, *63*, e202317638. [[CrossRef](#)]
39. Firaha, D.; Liu, Y.M.; van de Streek, J.; Sasikumar, K.; Dietrich, H.; Helfferich, J.; Aerts, L.; Braun, D.E.; Broo, A.; DiPasquale, A.G.; et al. Predicting Crystal Form Stability under Real-World Conditions. *Nature* **2023**, *623*, 324–328. [[CrossRef](#)] [[PubMed](#)]
40. Vušak, D.; Mišković Špoljarić, K.; Jurec, J.; Žilić, D.; Prugovečki, B. Ternary Coordination Compounds of Copper(II) with Glycine and 2,2'-Bipyridine: Synthesis, Structural Characterization, Magnetic and Biological Properties. *Croat. Chem. Acta* **2023**, *95*, 157–165. [[CrossRef](#)]
41. Vušak, D.; Ležaić, K.; Judaš, N.; Prugovečki, B. Ternary Copper(II) Coordination Compounds with Nonpolar Amino Acids and 2,2'-Bipyridine: Monomers vs. Polymers. *Crystals* **2024**, *14*, 656. [[CrossRef](#)]
42. Degen, T.; Sadki, M.; Bron, E.; König, U.; Nénert, G. The HighScore Suite. *Powder Diffr.* **2014**, *29*, S13–S18. [[CrossRef](#)]
43. *DataViewer*; Version 1.9a; PANalytical B.V.: Almelo, The Netherlands, 2018.
44. Wojciechowska, A.; Jezierska, J.; Bieńko, A.; Daszkiewicz, M. Structural and Spectroscopic Parameters of Distortion in [Cu(Bpy)<sub>2</sub>(O<sub>2</sub>SO<sub>2</sub>)]·CH<sub>3</sub>OH and [Cu(Bpy)<sub>3</sub>][SO<sub>4</sub>]·7.5H<sub>2</sub>O—Synthesis, Crystal Structure, Spectroscopic and Magnetic Properties. *Polyhedron* **2011**, *30*, 1547–1554. [[CrossRef](#)]
45. Fitzgerald, W.; Foley, J.; McSweeney, D.; Ray, N.; Sheahan, D.; Tyagi, S.; Hathaway, B.; O'Brien, P. Electronic Properties and Crystal Structure of (2,2'-Bipyridyl)-Catena- $\mu$ -(Oxalato-O<sup>1</sup>O<sup>2</sup>:O<sup>1</sup>O<sup>2</sup>)-Copper(II) Dihydrate and Aqua(2,2'-Bipyridyl)-(Oxalato-O<sup>1</sup>O<sup>2</sup>)Copper(II) Dihydrate. *J. Chem. Soc. Dalton Trans.* **1982**, 1117–1121. [[CrossRef](#)]

46. Castro, I.; Faus, J.; Julve, M.; Muñoz, M.C.; Diaz, W.; Solans, X. Study of the Interaction between [Cu(Bipy)]<sup>2+</sup> and Oxalate in Dimethyl Sulfoxide. Crystal Structure of [Cu<sub>2</sub>(Bipy)<sub>2</sub>(H<sub>2</sub>O)<sub>2</sub>ox]SO<sub>4</sub>·[Cu(Bipy)Ox]. *Inorganica Chim. Acta* **1991**, *179*, 59–66. [[CrossRef](#)]
47. Greenspan, L. Humidity Fixed Points of Binary Saturated Aqueous Solutions. *J. Res. Natl. Bur. Stand. A Phys. Chem.* **1977**, *81A*, 89. [[CrossRef](#)]
48. *CrysAlisPRO*; Version 171.42.63a; Rigaku Oxford Diffraction: Yarnton, UK, 2022.
49. Sheldrick, G.M. A Short History of SHELX. *Acta Crystallogr. A* **2008**, *64*, 112–122. [[CrossRef](#)]
50. Sheldrick, G.M. Crystal Structure Refinement with SHELXL. *Acta Crystallogr. C Struct. Chem.* **2015**, *71*, 3–8. [[CrossRef](#)]
51. Farrugia, L.J. WinGX and ORTEP for Windows: An Update. *J. Appl. Crystallogr.* **2012**, *45*, 849–854. [[CrossRef](#)]
52. Macrae, C.F.; Sovago, I.; Cottrell, S.J.; Galek, P.T.A.; McCabe, P.; Pidcock, E.; Platings, M.; Shields, G.P.; Stevens, J.S.; Towler, M.; et al. Mercury 4.0: From Visualization to Analysis, Design and Prediction. *J. Appl. Crystallogr.* **2020**, *53*, 226–235. [[CrossRef](#)]
53. Spek, A.L. Single-Crystal Structure Validation with the Program PLATON. *J. Appl. Crystallogr.* **2003**, *36*, 7–13. [[CrossRef](#)]
54. Blatov, V.A.; Shevchenko, A.P.; Proserpio, D.M. Applied Topological Analysis of Crystal Structures with the Program Package ToposPro. *Cryst. Growth Des.* **2014**, *14*, 3576–3586. [[CrossRef](#)]
55. Spackman, P.R.; Turner, M.J.; McKinnon, J.J.; Wolff, S.K.; Grimwood, D.J.; Jayatilaka, D.; Spackman, M.A. CrystalExplorer: A Program for Hirshfeld Surface Analysis, Visualization and Quantitative Analysis of Molecular Crystals. *J. Appl. Crystallogr.* **2021**, *54*, 1006–1011. [[CrossRef](#)] [[PubMed](#)]
56. Perin, N.; Nhili, R.; Cindrić, M.; Bertoša, B.; Vušak, D.; Martin-Kleiner, I.; Laine, W.; Karminski-Zamola, G.; Kralj, M.; David-Cordonnier, M.-H.; et al. Amino Substituted Benzimidazo[1,2-a]Quinolines: Antiproliferative Potency, 3D QSAR Study and DNA Binding Properties. *Eur. J. Med. Chem.* **2016**, *122*, 530–545. [[CrossRef](#)] [[PubMed](#)]
57. Pršir, K.; Horak, E.; Kralj, M.; Uzelac, L.; Liekens, S.; Steinberg, I.M.; Krištafor, S. Design, Synthesis, Spectroscopic Characterisation and In Vitro Cytostatic Evaluation of Novel Bis(Coumarin-1,2,3-Triazolyl)Benzenes and Hybrid Coumarin-1,2,3-Triazolyl-Aryl Derivatives. *Molecules* **2022**, *27*, 637. [[CrossRef](#)] [[PubMed](#)]
58. Gonnet, L.; Borchers, T.H.; Lennox, C.B.; Vainauskas, J.; Teoh, Y.; Titi, H.M.; Barrett, C.J.; Koenig, S.G.; Nagapudi, K.; Friščić, T. The “η-Sweet-Spot” (H<sub>max</sub>) in Liquid-Assisted Mechanochemistry: Polymorph Control and the Role of a Liquid Additive as Either a Catalyst or an Inhibitor in Resonant Acoustic Mixing (RAM). *Faraday Discuss.* **2023**, *241*, 128–149. [[CrossRef](#)]
59. Nakamoto, K. *Infrared and Raman Spectra of Inorganic and Coordination Compounds*; Wiley: Hoboken, NJ, USA, 2008; ISBN 9780471744931.

**Disclaimer/Publisher’s Note:** The statements, opinions and data contained in all publications are solely those of the individual author(s) and contributor(s) and not of MDPI and/or the editor(s). MDPI and/or the editor(s) disclaim responsibility for any injury to people or property resulting from any ideas, methods, instructions or products referred to in the content.